



Genesis of the Xifeng Low-Temperature Geothermal Field, Guizhou, SW China: Constrains From Geology, Element Geochemistry, and D-O Isotopes

Yanyan Li^{1,2*}, Ji Dor^{3,4}, Chengjiang Zhang³, Guiling Wang^{1,2}, Baojian Zhang^{1,2}, Fangfang Zhang⁵ and Yifei Xing^{1,2}

¹Chinese Academy of Geological Sciences, Beijing, China, ²MNR Laboratory of Deep Geosciences and Exploration Technology, Chinese Academy of Geological Sciences, Beijing, China, ³College of Earth Science, Chengdu University of Technology, Chengdu, China, ⁴Tibet Bureau of Geological Exploration, Lhasa, China, ⁵State Key Laboratory of Geological Processes and Mineral Resources, China University of Geosciences, Beijing, China

OPEN ACCESS

Edited by:

Yinhui Zuo,
Chengdu University of Technology,
China

Reviewed by:

Wei Xu,
Xi'an Jiaotong University, China
Xiaoyin Tang,
Chinese Academy of Geological
Sciences, China

*Correspondence:

Yanyan Li
liyanyan@cags.ac.cn

Specialty section:

This article was submitted to
Economic Geology,
a section of the journal
Frontiers in Earth Science

Received: 25 September 2021

Accepted: 19 November 2021

Published: 24 December 2021

Citation:

Li Y, Dor J, Zhang C, Wang G, Zhang B, Zhang F and Xing Y (2021) Genesis of the Xifeng Low-Temperature Geothermal Field, Guizhou, SW China: Constrains From Geology, Element Geochemistry, and D-O Isotopes. *Front. Earth Sci.* 9:782943. doi: 10.3389/feart.2021.782943

The Xifeng geothermal field is located in the Yangtze Craton, SW China, and is one of the most representative low-temperature geothermal fields in China. Widespread thermal anomalies, hot springs, and geothermal wells have been reported by previous studies. However, the nature and forming mechanisms of the field remain poorly understood. Element geochemical (ions, rare earth elements) and stable isotopic (D, O) composition of hot springs, geothermal fluids, rivers, and cold springs from different locations of the Xifeng geothermal field were analyzed in this study. The ions studies revealed that most samples featured the Ca-Mg-HCO₃ type, except Xifeng hot springs, and which were characterized by the Ca-Mg-HCO₃-SO₄ type. Based on quartz geothermometers, the estimated reservoir temperature was 77°C. The results of stable isotopes (D, O) manifest that the Xifeng geothermal system was recharged by meteoric water at an elevation of 1,583 m from SW to NE. The research of rare earth elements (REE) revealed that their accumulation characteristics and obvious positive Eu anomaly were inherited from host feldspar-bearing reservoir dolomites through water-rock interactions. Combined with these observations, geological setting, and previous studies, it was concluded that the formation of the Xifeng geothermal field resulted from recharge, deep circulation, and secondary rising of the meteoric water along the faults. First, meteoric water infiltrated to depth through faults and crack zones. Second, the deep-infiltrated water was heated by radioactive heat, deep heat, and tectonic frictional heat. Finally, as the warmed-up waters underwent considerable deep circulation in the reservoir, it rose again along the main faults, and mixed with groundwater near the surface. Taken together, we suggest that the Xifeng geothermal system should be assigned as a faults-controlling, and deeply circulating meteoric water of low-temperature category.

Keywords: geology, element geochemistry, D-O isotopes, xifeng, SW China

INTRODUCTION

Geothermal resources are well developed in China and contribute significantly to the global supply of total resources (7.9%; Wang G. L. et al., 2017), while they are mainly produced as widespread medium-low temperature types (Wang G. L. et al., 2017; Li and Wang 2015). The occurrence of high-temperature types is limited and mainly formed in South China, e.g., southern Tibet, western Sichuan and Yunnan, as well as the south-east coastal area (Duo, 2003; Guo et al., 2007; Zhang et al., 2016; Guo et al., 2017a, b; Tian et al., 2018; Cheng et al., 2021; Zheng et al., 2021). These distribution characteristics mean that research on geothermal resources in South China mainly focuses on the high-temperature type, whereas studies on the medium-low type are limited.

South China has a significant geothermal potential and hosts many world-famous geothermal fields, including high-temperature Yangbajing, Tengchong, and Kangding, as well as low-temperature Xifeng in Guizhou Province (Guo and Wang, 2012; Guo et al., 2014; Li et al., 2018; Wang et al., 2018; Yang et al., 2018; Wang et al., 2019b; Li J. et al., 2021). There are lots of hot springs, hydrothermal manifestations, and geothermal wells located in the Xifeng geothermal field, indicating great potential for exploration, and utilized prospects (Yang et al., 2018; **Figure 1B**). Although systematic exploration and utilization of Xifeng began in the 1950s, the scientific research on the overall field is poor, and attributed to the single application mode of geothermal resources. In recent years, with the increased need for renewable energy, a new round of exploration work and scientific study has been conducted to

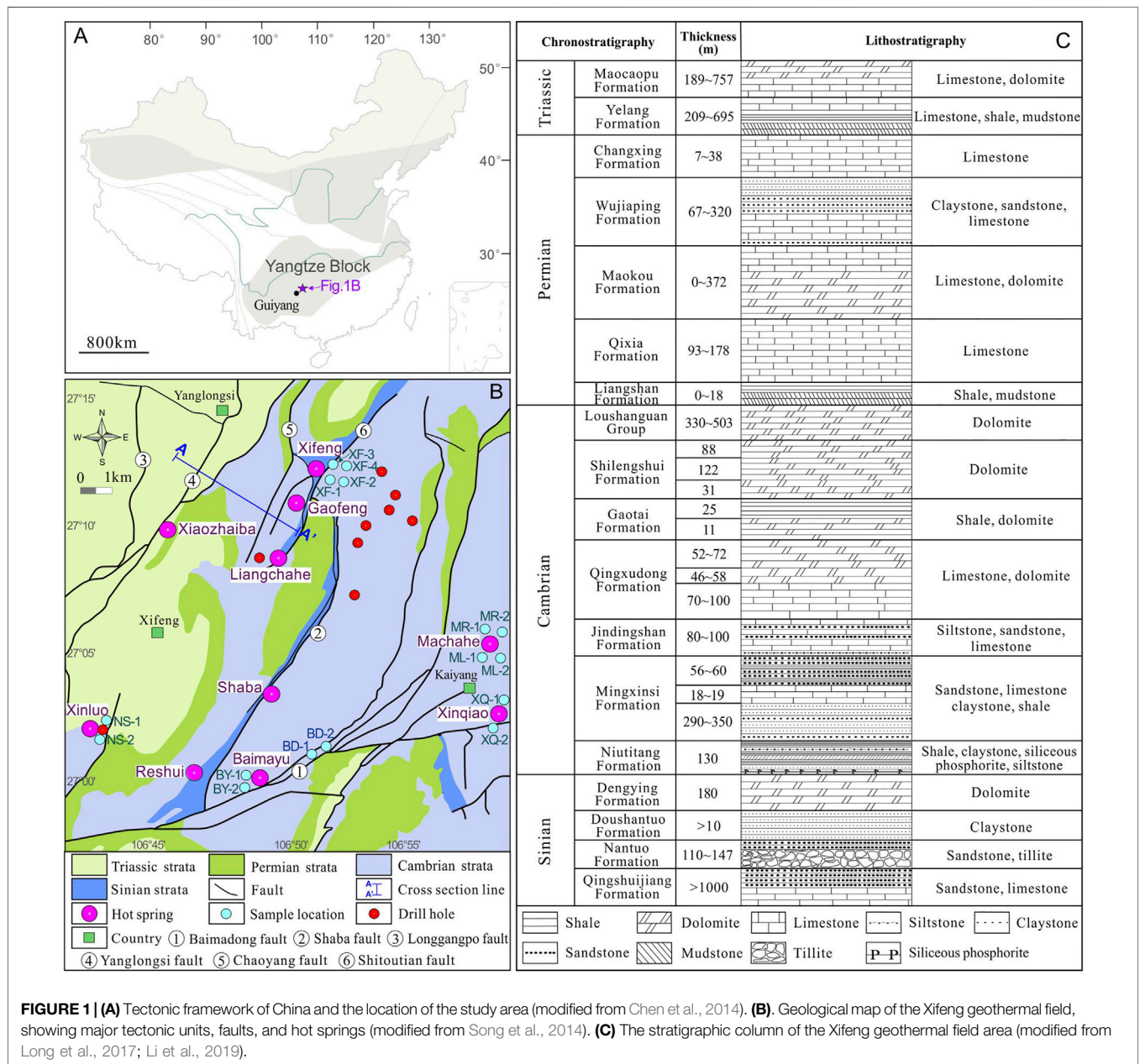


FIGURE 1 | (A) Tectonic framework of China and the location of the study area (modified from Chen et al., 2014). **(B)** Geological map of the Xifeng geothermal field, showing major tectonic units, faults, and hot springs (modified from Song et al., 2014). **(C)** The stratigraphic column of the Xifeng geothermal field area (modified from Long et al., 2017; Li et al., 2019).

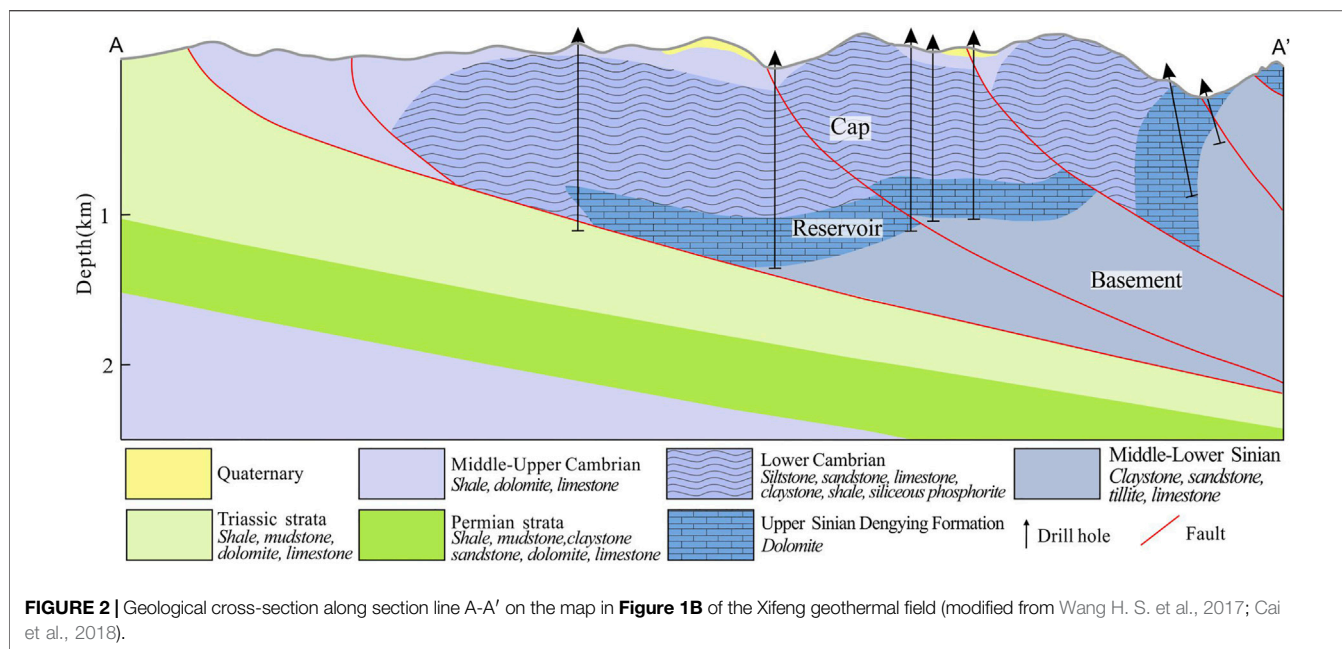


TABLE 1 | Geothermometry equations (in°C) for the cation and silica geothermometers used in this study.

Geothermometer	Reference	Equations
Na-K	Fournier, (1979)	$T = 1,217/[\log(\text{Na}/\text{K})+1.483]-273.15$
Na-K	Truesdell, (1976)	$T = 856/[\log(\text{Na}/\text{K})+0.857]-273.15$
Na-K	Giggenbach and Goguel, (1988)	$T = 1,390/[\log(\text{Na}/\text{K})+1.75]-273.15$
Na-K	Tonani, (1980)	$T = 883/[\log(\text{Na}/\text{K})+0.78]-273.15$
Na-K	Nieva and Nieva (1987)	$T = 1,178/[\log(\text{Na}/\text{K})+1.47]-273.15$
Na-K	Arnórsson, (1983)	$T = 933/[\log(\text{Na}/\text{K})+0.993]-273.15$
Na-K	Arnórsson, (1983)	$T = 1,319/[\log(\text{Na}/\text{K})+1.699]-273.15$
Na-K	Michard et al. (1979)	$T = 908/[\log(\text{Na}/\text{K})+0.7]-273.15$
K-Mg	Giggenbach et al. (1983)	$T = 4,410/[14-\log(\text{K}^2/\text{Mg})]-273.15$
Na-K-Ca	Fournier and Truesdell, (1973)	$T = 1,647/[\log(\text{Na}/\text{K})+b\log(\text{Ca}^{1/2}/\text{Na})+2.06]+2.47]-273.15$, where $b = 4/3$, if $T < 100^\circ\text{C}$; $b = 1/3$, if $T > 100^\circ\text{C}$
Quartz, no steam loss (conductive)	Fournier, (1977)	$T = [1,309/(5.19-\log\text{SiO}_2)]-273.15$
Quartz, maximum steam loss at 100°C (adiabatic)	Fournier, (1977)	$T = [1,522/(5.75-\log\text{SiO}_2)]-273.15$
Chalcedony (no loss of steam)	Fournier, (1992)	$T = [1,032/(4.69-\log\text{SiO}_2)]-273.15$
Chalcedony (maximum steam loss)	Fournier, (1977)	$T = [1,264/(5.31-\log\text{SiO}_2)]-273.15$
α-Cristobalite	Fournier, (1977)	$T = [1,000/(4.78-\log\text{SiO}_2)]-273.15$
β-Cristobalite	Fournier, (1977)	$T = [781/(4.51-\log\text{SiO}_2)]-273.15$

evaluate the potential of hydrothermal resources. Previous studies have focused on single hot springs or geothermal wells mainly based on hydrogeochemistry and geology (Li and Shen, 2014; Song et al., 2014; Cai et al., 2018). However, comprehensive comparative research on respective hot springs, geothermal wells, and related rivers from the whole geothermal field have not been conducted, meaning that the signature, evolution, and forming mechanisms of the Xifeng geothermal field remain obscure.

In this study, representative hot springs, geothermal fluids, cold springs, and related river waters were sampled for detailed element geochemistry (ions, rare earth elements) and stable isotopes (D, O) studies. This new comprehensive dataset allows us to confirm the

feature, evolution, and genesis of the geothermal fluids, which will provide a favorable understanding of the forming mechanisms for the Xifeng geothermal field, and similar geothermal fields in South China and worldwide.

GEOLOGICAL TECTONIC AND HYDROGEOLOGICAL SETTINGS

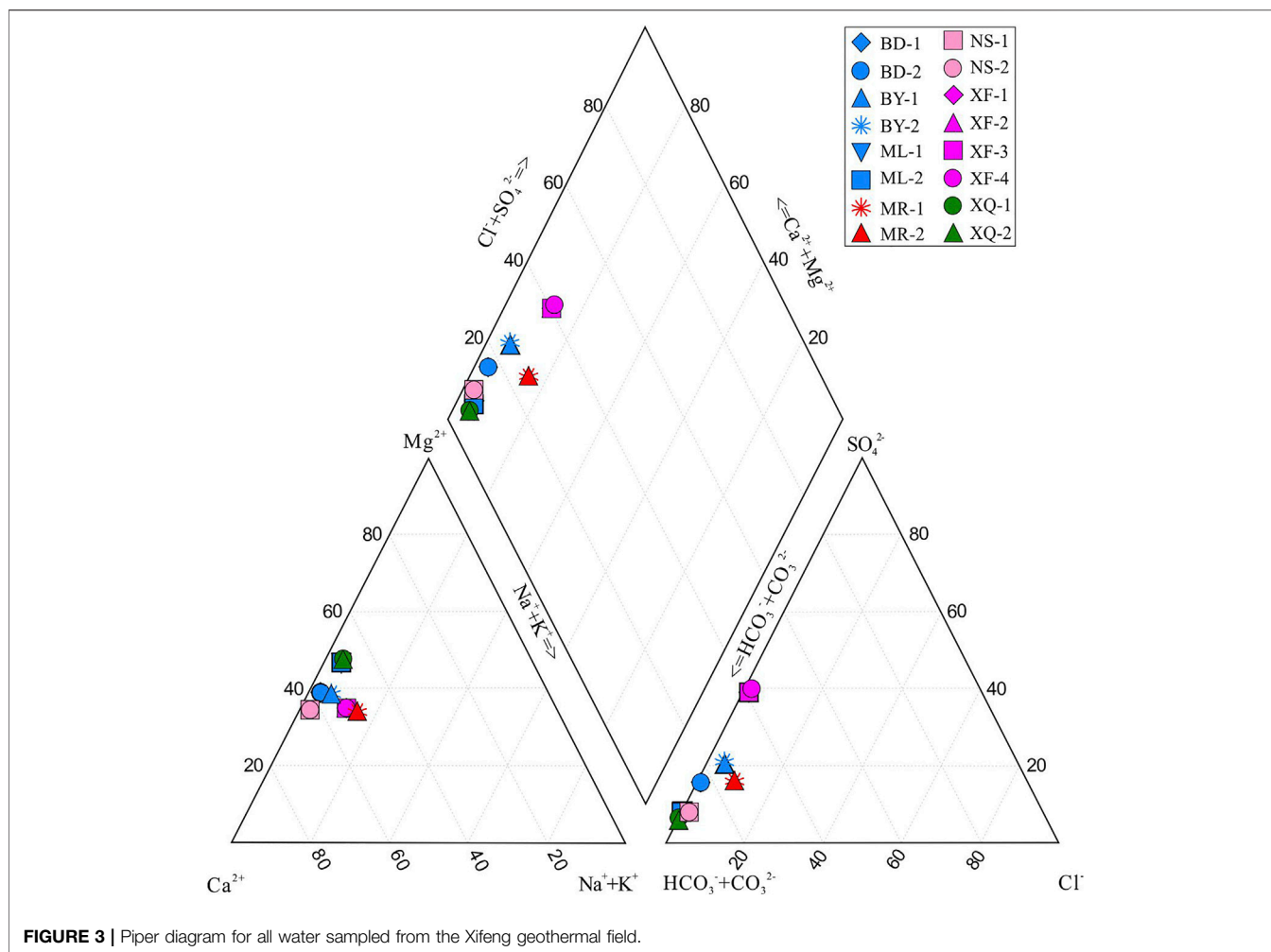
Geological Setting

The Xifeng geothermal field is situated in the central Guizhou Province, southwestern China (**Figure 1A**). The geological

TABLE 2 | Measured parameters, major ion chemistry (mg/L), SiO₂ (mg/L), Rare Earth Element (μg/L), and δD-δ¹⁸O composition of water samples from the Xifeng geothermal field.

Sample NO.	BY-1	BY-2	BD-1	BD-2	MR-1	MR-2	ML-1	ML-2	XQ-1	XQ-2	XF-1	XF-2	XF-3	XF-4	NS-1	NS-2
PH	8.05	7.98	8.06	8.12	8.01	7.92	7.83	7.96	8.19	8.15	8.05	8	8.08	8.05	8.06	8.19
δ ¹⁸ O _{V-SMOW} (‰)	-7.5	-8.1	-8.2	-8.1	-7.8	-8.3	-7.4	-7	-6.5	-7	-8	-8.5	-8.3	-7.9	-9.2	-8.7
δD _{V-SMOW} (‰)	-51.1	-53.7	-54.1	-55.6	-56.2	-57.4	-48.3	-47.9	-45.9	-47.7	-56.3	-59.1	-58.8	-58	-65.6	-65.6
T(°C)	12	12	13	13	43	43	14	14	14	14	56	56	56	56	48	48
K ⁺	1.2	1.13	2.23	2.17	1.04	1.08	7.96	7.64	2.2	2.16	3.51	3.41	3.56	3.7	3.08	2.98
Na ⁺	1.86	1.81	4.66	4.71	4.27	4.33	16	15.9	1.67	1.68	11.7	11.8	11.8	12.3	2.29	2.12
Ca ²⁺	34.7	35.1	47.2	49	45.1	44.6	62.1	61.2	57.2	57.3	52.7	52.5	52.8	54.3	36.9	36.9
Mg ²⁺	14.3	14.3	20.2	20.7	26.2	26	25	24.9	19.1	19.3	21.1	20.9	21.1	21.6	22.1	22.1
HCO ₃ ⁻	140	141	184	184	245	245	235	235	232	234	169	172	171	170	208	209
SO ₄ ²⁻	20.5	20.8	39.6	40.4	17.6	16.6	41.5	40.1	16.5	16.6	88.4	91.5	88.3	91.4	10.7	10.4
Cl ⁻	1.35	1.33	7.02	7.08	0.67	0.654	18.4	18	3.16	3.23	3.07	3.03	3.04	3.11	0.725	0.725
SiO ₂	4.68	4.61	6.54	6.58	20.43	20.46	5.89	5.93	6.34	6.23	39.71	39.92	39.85	38.82	15.39	15.79
La	0.01	0.005	0.008	0.005	0.006	0.006	0.013	0.01	0.022	0.018	0.082	0.006	<0.002	<0.002	0.002	0.003
Ce	0.012	0.011	0.013	0.013	0.002	<0.002	0.022	0.024	0.043	0.048	0.097	0.006	0.002	0.005	0.003	0.004
Pr	0.002	0.003	<0.002	0.002	<0.002	<0.002	0.002	0.002	0.006	0.005	<0.002	<0.002	<0.002	<0.002	<0.002	0.002
Nd	0.008	0.003	0.158	0.006	0.011	0.003	0.016	0.008	0.024	0.049	0.002	0.005	0.002	0.004	0.002	0.006
Sm	<0.002	0.003	0.002	0.002	0.004	0.007	0.002	0.004	0.008	0.004	0.002	0.002	<0.002	<0.002	<0.002	0.002
Eu	0.007	0.004	0.004	0.012	0.027	0.03	0.016	0.006	0.005	0.002	<0.002	0.01	0.005	0.016	0.012	0.015
Gd	0.003	0.006	<0.002	0.004	0.002	0.005	0.011	0.013	0.005	0.005	0.003	0.005	<0.002	0.002	0.006	0.003
Tb	<0.002	<0.002	<0.002	<0.002	<0.002	0.007	<0.002	<0.002	<0.002	<0.002	<0.002	<0.002	<0.002	<0.002	<0.002	<0.002
Dy	0.003	<0.002	<0.002	0.003	<0.002	<0.002	0.004	0.002	0.007	<0.002	<0.002	<0.002	<0.002	<0.002	<0.002	0.004
Y	0.022	0.015	0.006	0.011	0.006	0.006	0.018	0.012	0.024	0.031	0.01	0.012	0.008	0.008	0.005	0.006
Ho	<0.002	<0.002	<0.002	<0.002	<0.002	<0.002	<0.002	<0.002	<0.002	0.002	<0.002	<0.002	<0.002	<0.002	<0.002	0.002
Er	0.002	0.005	<0.002	0.002	<0.002	0.002	0.005	<0.002	0.003	<0.002	<0.002	0.002	<0.002	<0.002	<0.002	0.002
Tm	0.002	<0.002	<0.002	<0.002	<0.002	<0.002	<0.002	<0.002	<0.002	<0.002	<0.002	<0.002	<0.002	<0.002	<0.002	<0.002
Yb	0.004	<0.002	0.007	0.002	<0.002	<0.002	<0.002	<0.002	0.002	0.002	<0.002	<0.002	<0.002	<0.002	0.002	0.002
Lu	0.002	<0.002	<0.002	<0.002	<0.002	<0.002	<0.002	<0.002	<0.002	<0.002	<0.002	<0.002	<0.002	<0.002	<0.002	<0.002
Total REE	<0.083	<0.067	<0.214	<0.07	<0.074	<0.08	<0.119	<0.093	<0.157	<0.176	<0.214	<0.062	<0.039	<0.055	<0.048	<0.057
δEu	>13.457	4.440	>9.418	19.978	44.950	23.878	16.063	3.918	3.723	2.106	<3.845	14.891	>11.772	>37.671	>16.312	28.836
δCe	0.619	0.655	>0.750	0.949	>0.133	0.133	0.995	1.238	0.864	1.167	>1.748	>0.400	0.231	0.577	>0.346	0.377
Sample type	River	River	River	River	Hot spring	Hot spring	River	River	Cold spring	Cold spring	Hot spring	Hot spring	Hot spring	Hot spring	Well	Well
Water type	Ca-Mg-HCO ₃ -SO ₄	Ca-Mg-HCO ₃	Ca-Mg-HCO ₃													

Notes: δEu = Eu/N/sqrt(Sm*N*Gd/N); δCe = Ce/N/sqrt(La*N*Pr/N); N=Post-Archean Shale normalized; LREE = La + Ce + Pr + Nd + Sm + Eu; HREE = Gd + Tb + Dy + Ho + Er + Tm + Yb + Lu.



location is in the Guiyang Complex Tectonic Deformation Zone related to the central Guizhou uplift within the Yangtze Craton in South China (Figure 1A; Ling et al., 2015, 2017; Long et al., 2017; Li et al., 2019, Li Y. Y. et al., 2021). The basement is made of Meso- to Neoproterozoic metamorphosed marine sedimentary rocks. The cover consists of Neoproterozoic (Sinian) to Triassic marine sedimentary rocks and Jurassic terrestrial sedimentary rocks, which underwent multiple Phanerozoic tectono-thermal activities (Li et al., 2019; Li J. et al., 2021).

The stratigraphic succession of the Xifeng geothermal field consists of, from bottom to top, the Sinian Qingshuijiang, Nantuo, Doushantuo, and Dengying formations, lower Cambrian Niutitang, Mingxinsi, Jindingshan, Qingxudong, Gaotai, and Shilengshui formations and Loushanguan Group, Permian Liangshan Qixia, Maokou, Wujiaping, and Changxing formations, and Triassic Yelang and Maocaopu formations (Figure 1C; Ling et al., 2015; Long et al., 2017; Li et al., 2019). The Dengying, Qingxudong, Gaotai, and Shilengshui formations and Loushanguan Group are made of carbonates, dominantly dolomite. The Qingshuijiang and Nantuo formations consist of sandstone intercalated with limestone and tillite, respectively. The Doushantuo Formation is made of claystone. The Niutitang

Formation is comprised of shale, claystone, siliceous phosphorite, and siltstone, and the Mingxinsi Formation comprises sandstone, limestone, claystone, and shale. The Jindingshan Formation consists of siltstone, sandstone, and limestone. The Permian rocks consist of shale and mudstone (Liangshan Formation), limestone (Qixia and Changxing Formations), dolomite and limestone (Maokou Formation), and claystone, sandstone, and limestone (Wujiaping Formation). The Triassic rocks are made of limestone, shale, and mudstone (Yelang Formation), and carbonate, i.e., limestone and dolomite (Maocaopu Formation) (Ling et al., 2015; Ji, 2015; Long et al., 2018, 2019).

The central Guizhou region experienced a series of tectonic events from Sinian to late Cambrian, such as the Yunan Movement (forming the central Guizhou uplift; Mei et al., 2005; Ling et al., 2015; Long et al., 2017), Duyun and Guangxi Movements (uplifting the central Guizhou; Yu and Wang, 1995; Long et al., 2018), and Dongwu Movement as well as a late Permian Emeishan mantle-plume eruption event (Zhou et al., 2002; He et al., 2005; Jian et al., 2009). These tectonic activities resulted in widespread folding and faulting in the study area, especially the followed Indosinian orogeny, Yanshanian, and

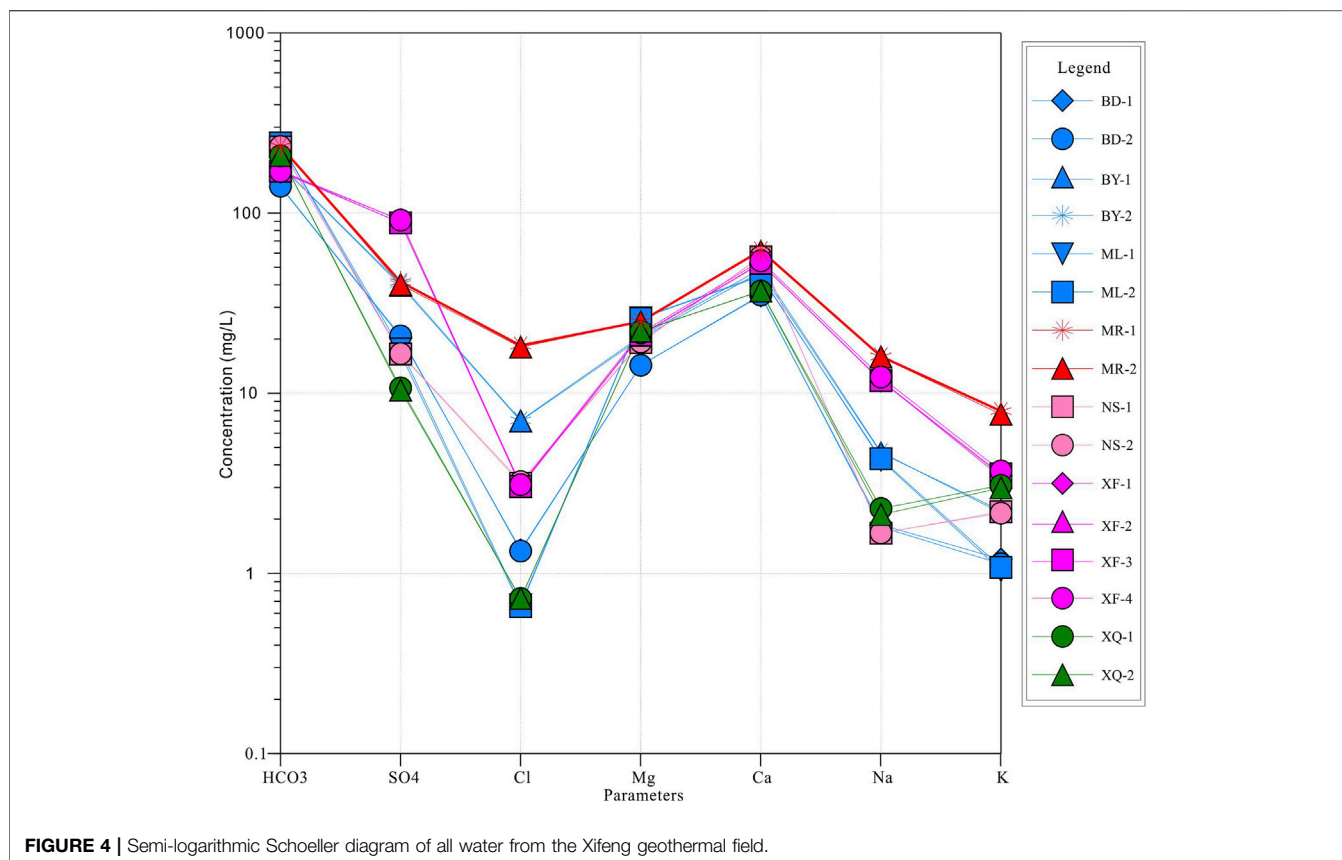


FIGURE 4 | Semi-logarithmic Schoeller diagram of all water from the Xifeng geothermal field.

Himalayan movements (Huang, 1945; Wang and Mo, 1995; Carter et al., 2001; Chen, 2005; Reid et al., 2007; Li J. et al., 2021), which controlled the distribution of geothermal resources.

Tectonic Setting

Faults are well developed in the study area due to multi-stage tectonic activities, such as the Emeishan mantle-plume eruption, Yanshanian orogeny, and Himalayan crust uplift movement (Figure 1B). These faults are mainly thin-skinned with high hydraulic conductivities and resulted in greater exploitation potential relative to other geothermal fields in China. One of the most important faults is the compresso-shear strike-slip Baimadong fault, which is the main conduit and connects the deep heat source (He et al., 2014; Li and Shen, 2014). The fault is around 50 km long, ENE-trending and dipping to SE at angles of 75° towards 90°, and assigned to a regional large-scale deep fault (Figure 1B; Zhang et al., 2017; Li et al., 2019, Li J. et al., 2021). In addition, secondary Neoid active faults such as the Shaba, Chaoyang, and Shitoutian faults are developed within the tectonic system and act as heat transporting channels (Figure 1B; Song et al., 2014). Among them, the Shaba fault is NE-trending and dipping to SE at angle of 70°. The Chaoyang fault is parallel to the Shaba fault with a length of ~20 km, NE-trending and dipping to SE at angles of 50° towards 70°. The Shitoutian fault with a NW orientation dips to NE at angles of 75° (Ji, 2015). The fault kinematics and orientations control the distribution of geothermal resources in the study region.

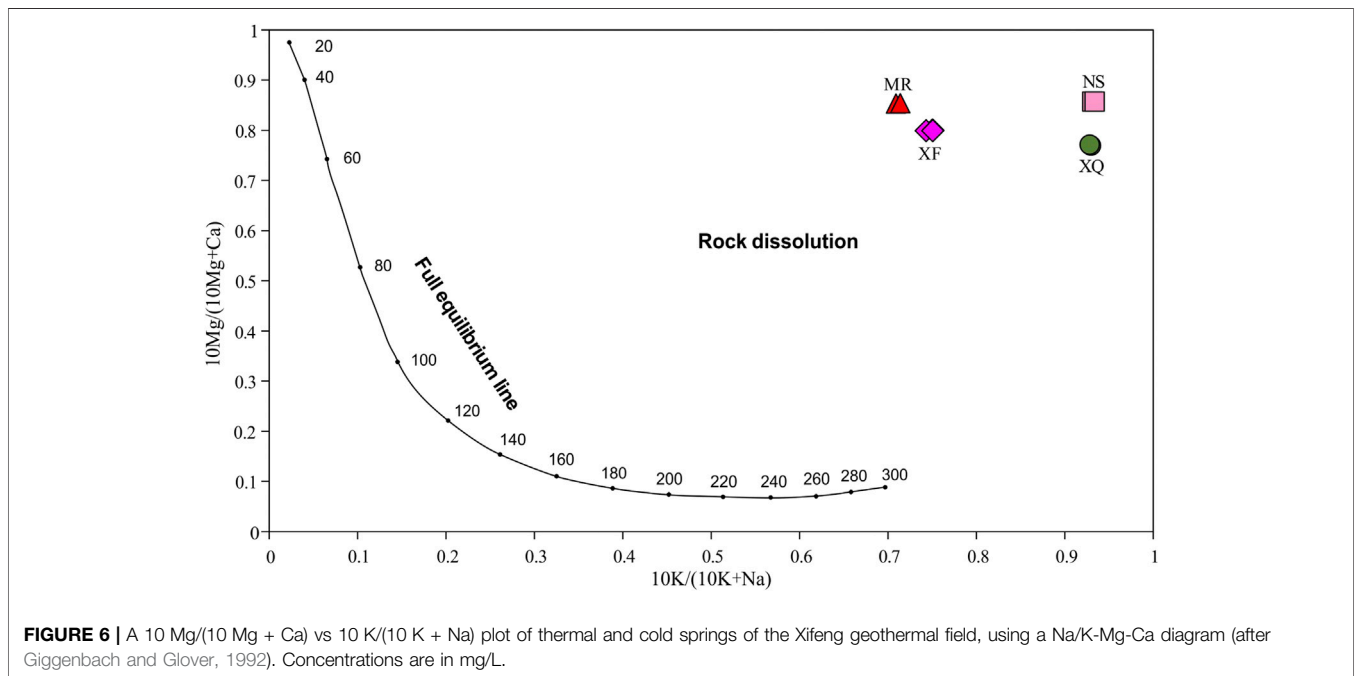
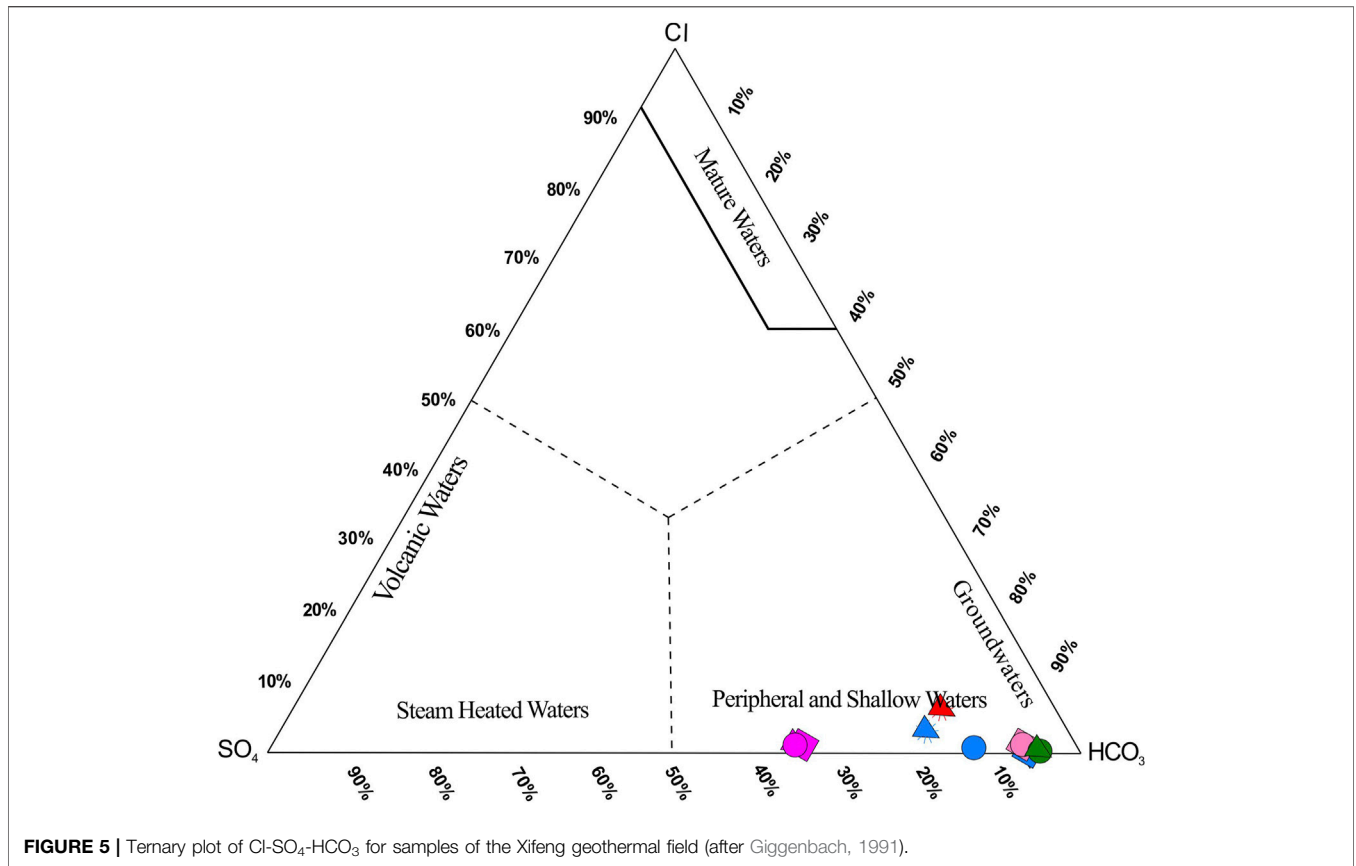
Hydrogeological Setting

The Xifeng geothermal field covers an area of 102.7 km² (Luo, 2020). Approximately 250 exploration and production geothermal wells have been drilled in this area since the 1950s, and the deepest depth is 2,500 m (He et al., 2014; Yang et al., 2018). Moreover, there are numerous hot springs within this area, including the famous Xifeng hot spring. The measured temperature ranges from 39 to 42°C in the Baimadong area to 53–56°C in the Xifeng area (Luo, 2020). The geothermal gradient of the study area is 2.5–3.0°C/hm with the heat flow rate varying from 50 to 75 mW/m² (Song et al., 2014; Wang et al., 2019a). The Dengying Formation is the main reservoir and the upper Jindingshan, Mingxinsi, and Niutitang formations form the cap of the geothermal system (Figure 2; He et al., 2014; Li and Shen, 2014; Song et al., 2014; Cai et al., 2018).

SAMPLING AND STUDY METHODS

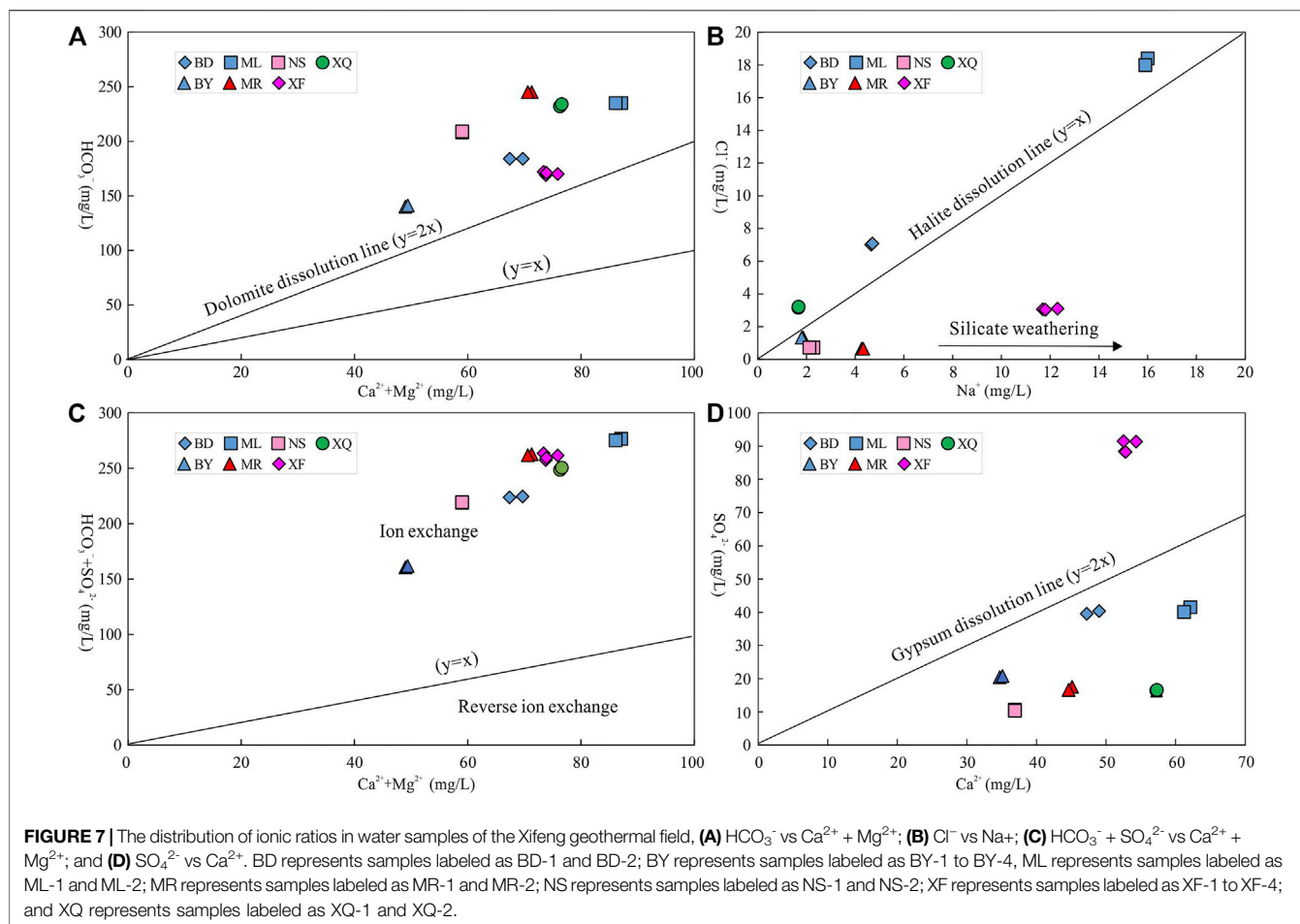
Water Sample and Analyses

Fieldwork was carried out in the Xifeng area for collecting samples and obtaining relevant field data in April 2021. A total of 16 water samples (six hot spring samples, two geothermal well samples, six river samples, and two cold spring samples) at Xifeng were collected for major ions, REE, and D-O isotope analyses. Sample locations are shown in Figure 1B.



Time sensitive parameters were tested on site using a portable water quality analyzer. Samples were stored in new 500 ml polyethylene bottles that were rinsed with deionized water

twice before sampling. All mentioned hydrochemical analyses of the water samples were performed in the Laboratory of Beijing Research Institute of Uranium Geology. Samples used for analysis



of cations were acidified after collection through adding Suprapur HNO_3 to bring the pH to below 2. Analysis of major anions and cations was conducted by using Dionex ICS 1100 ion chromatography through Dionex ionpac AS-19HC and CS12A (4 mm \times 250 mm) columns, respectively. The analysis of rare earth elements in water samples was documented using a Thermo Scientific ELEMENT XR inductively coupled plasma mass spectrometer (ICP-MS). The instrument was externally calibrated using a multielement standard solution before ICP-MS analysis. The analytical precision was better than 10% for duplicate analysis of the samples. The composition of deuterium (D) and oxygen (^{18}O) isotopes of collected water samples was analyzed by a MAT 253 mass spectrometer in a continuous flow mode using a Gas-bench II preparation and introduction system. Isotopic data are expressed in the delta (δ) notation as the per mil (‰) deviation relative to the Standard Mean Ocean Water (SMOW); the analytic precisions (1σ) are ± 1.0 and $\pm 0.1\%$ for δD and $\delta^{18}\text{O}$, respectively.

Geothermometry

Chemical geothermometers are helpful to estimate the reservoir equilibrium temperature of the geothermal system by using the distribution and relative contents of various chemical indicators (i.e., dissolved silica, cation, gas, and isotopes; Das et al., 2021;

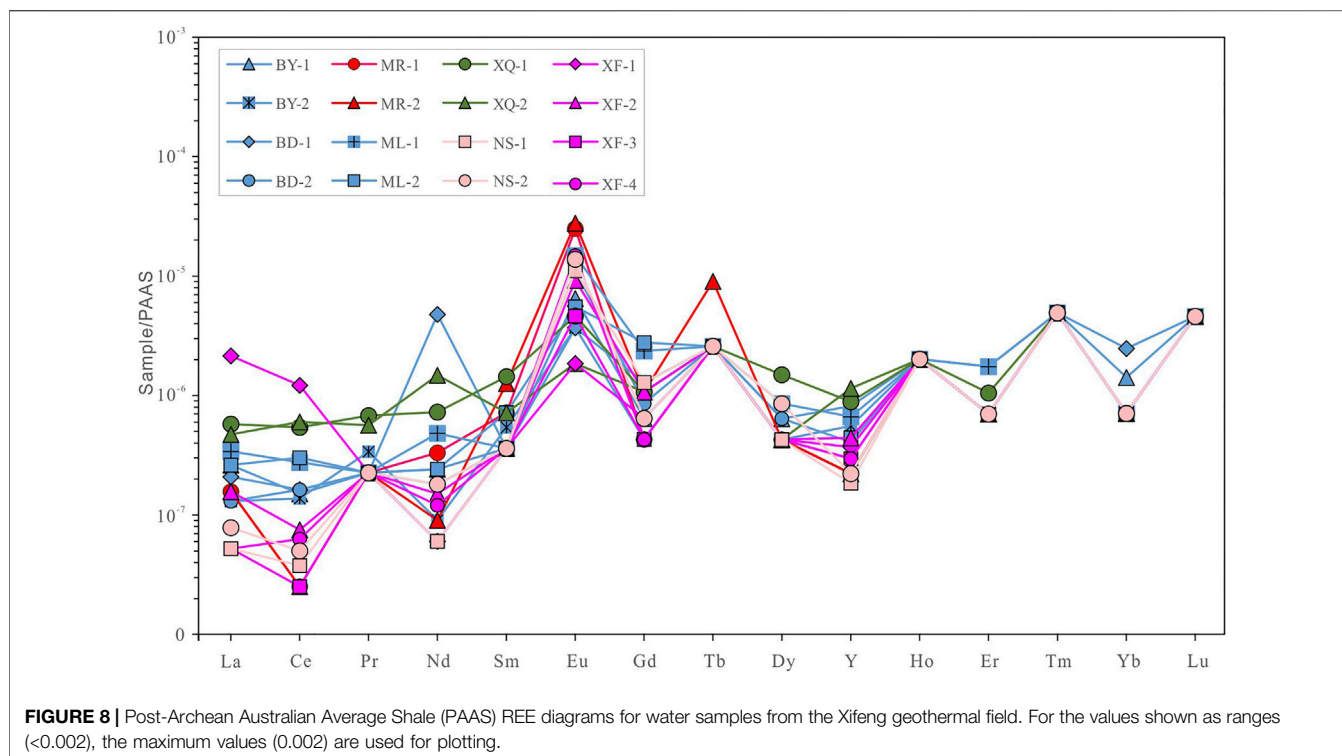
Saibi et al., 2021). Among them, temperature-dependent solubility (silica) and ion-exchange reactions (i.e., Na-K, Na-K-Ca) are the most applied (Das et al., 2021).

Various geothermometers can obtain different estimated reservoir temperatures as each geothermometer documents the last equilibrium of a specific chemical element and is directly affected by processes of boiling, dilution, and precipitation. Cation geothermometers (Na-K, K-Mg, and Na-K-Ca) and silica geothermometers (quartz no steam loss, quartz maximum steam loss, chalcedony no steam loss, chalcedony maximum steam loss, α -cristobalite, and β -cristobalite) applied in this study are shown in **Table 1**.

RESULTS

Ions Characteristics

The physico-chemical compositions of samples in this study are shown in **Table 2**. All samples showed alkaline pH values. In almost all the samples, the anions were dominated by HCO_3^- and the order of abundance was: $\text{HCO}_3^- > \text{SO}_4^{2-} > \text{Cl}^-$. Among the cations, the main ion was Ca^{2+} , and the following order of abundance was $\text{Ca}^{2+} > \text{Mg}^{2+} > \text{Na}^+ > \text{K}^+$. As shown in the Piper (1944) diagram (**Figure 3**), the waters were mostly



the Ca-Mg-HCO₃ type except the Xifeng hot spring water (Ca-Mg-HCO₃-SO₄). Waters had a similar varied pattern for concentrations of the cations and anions, except the high SO₄ contents (88.3–91.5 mg/L, avg. = 89.9 mg/L) in the Xifeng hot spring as illustrated in the Schoeller (1995) semi-logarithmic diagram (Figure 4). The ternary plot of Cl-SO₄-HCO₃ (Giggenbach, 1991) was conducted to evaluate the type of water mixed in thermal or non-thermal fluids, notably the peripheral waters involved are shown in Figure 5. The groundwater reacted with host rocks though the unequilibrated state (Figure 6). The intercorrelation of ions during the process of the water-rock reaction is shown in Figure 7.

Rare Earth Elements

The REE signatures of geothermal fluids can be used to assess the influences of water-rock interaction. REE composition of sampled waters were analyzed in this study, and the results are shown in Table 2. Four types of water appeared to have similar PAAS-normalized REE patterns, which were featured by heavy rare earth elements (HREE) enrichment compared to light rare earth elements (LREE), and positive Eu anomalies (Figure 8). The total rare earth elements (REE) contents in the geothermal well fluids (~0.048 to ~0.057 µg/L), hot spring waters (~0.039–~0.214 µg/L), river waters (~0.067 to ~0.214 µg/L), and cold spring waters (~0.157 to 0.176 µg/L) were relatively low. The δCe values were 0.346–0.377, 0.133–0.577, 0.619–0.238, and 0.864–1.167, and δEu values were 16.312–28.836, 3.845–44.950, 3.918–19.978, and 2.106–3.723 for waters of the geothermal well, hot spring, river, and cold spring, respectively.

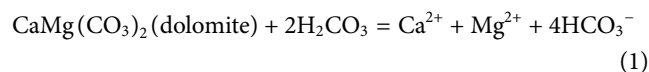
Hydrogen and Oxygen Isotope Compositions

Hydrogen and oxygen isotopic compositions of sampled waters in this study are shown in Table 2. The measured δD_{v-SMOW} values ranged from –65.6 to –65.6‰ (avg. = –65.6‰, n = 2), –59.1 to –56.2‰ (avg. = –57.6‰, n = 6), –55.6 to –47.9‰ (avg. = –51.8‰, n = 6), and –47.7 to –45.9‰ (avg. = –46.8‰, n = 2) for the geothermal well, hot springs, river, and cold spring waters, respectively. The measured δ¹⁸O_{v-SMOW} values were –9.2 to –8.7 (avg. = –8.95‰, n = 2), –8.5 to –7.8‰ (avg. = –8.13‰, n = 6), –8.2 to –7‰ (avg. = –7.71‰, n = 6), and –7 to –6.5‰ (avg. = –6.75‰, n = 2) for the geothermal well, hot spring, river, and cold spring waters, respectively.

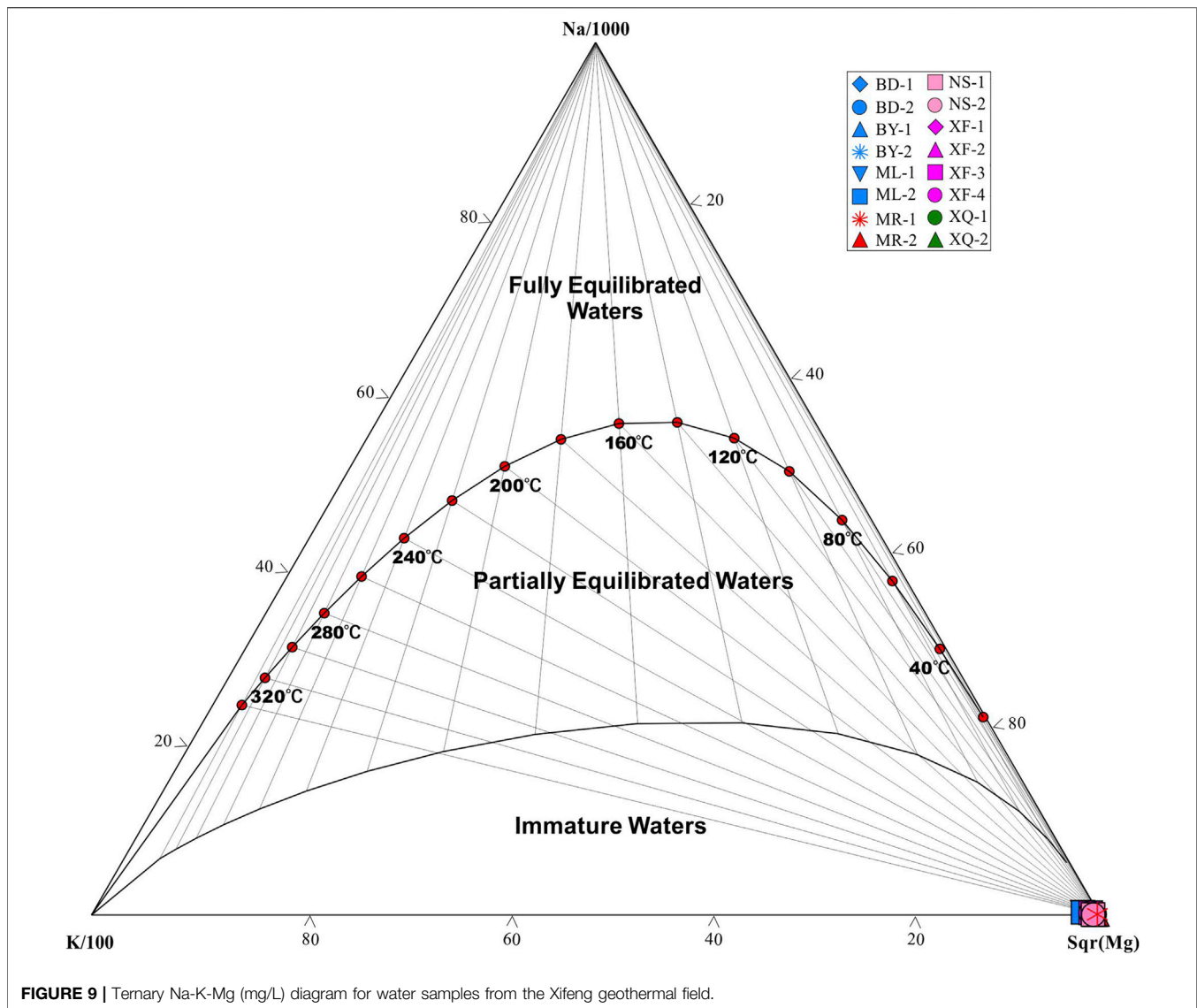
DISCUSSION

Source of Major Ions in the Geothermal Waters

Since most sampled waters were assigned to the Ca-Mg-HCO₃ type (Figure 3), this bicarbonate and Ca-Mg dominated feature can be attributed to the interaction with reservoir rocks, which are mainly Sinian dolomites. Ca²⁺, Mg²⁺, and HCO₃[–] were sourced from the dissolution of dolomites following the equation of



As illustrated in Figure 6, the water-rock interaction is a dominant process in thermal and cold springs of the Xifeng



geothermal field, although water is not equalized with the host reservoir rocks. Water-rock reactions can be further evidenced by the $\delta^{18}\text{O}$ results of geothermal waters, which deviate 2‰ of units from LMWL (Figure 11; Taylor, 1977). Additionally, most REE concentrations of sampled waters were above the detection limits (Table 2), indicating that REE in the samples were not derived from meteoric waters (Lewis et al., 1994). The positive Eu anomaly (triggered by the interaction between water and feldspar-bearing rocks or the physicochemical conditions; Sverjensky, 1984; Şener et al., 2017) supports the opinion that REE in the samples were inherited from feldspar-bearing dolomites through the water-rock interaction since the temperatures of geothermal fluids were much lower than 200°C (Figure 8; Sverjensky, 1984).

The characteristics of major ions and their intercorrelation can be used to deduce the geochemical processes caused by the water-rock reaction that the groundwater encounters along its flow path (Adams et al., 2001). According to Eq. 1, the dissolution of

dolomite would produce a $(\text{Ca}^{2+} + \text{Mg}^{2+})/\text{HCO}_3^-$ molar ratio of 1:2 (Han et al., 2013; Belkhiri and Narany, 2015). However, the ratios of $(\text{Ca}^{2+} + \text{Mg}^{2+})/\text{HCO}_3^-$ were lower than 0.5 (Figure 7A), indicating that other sources of HCO_3^- were involved in the geothermal fluids (e.g., silicate weathering), whereas the deficit in contents of Ca^{2+} and Mg^{2+} should be influenced by other hydrochemical processes (e.g., ion-exchange reaction), rather than the sole dissolution of dolomite. The affection of silicate weathering can also be inferred from the high values of $\text{Ca}^{2+}/\text{Mg}^{2+}$ (>1) in this study (Katz et al., 1997). Moreover, the Na^+/Cl^- molar ratios of the thermal waters were much higher than 1, further confirming the fact that the excess Na^+ was sourced from silicate weathering (Figure 7B; Bob et al., 2015). The plots for most samples were well above the 1:1 line of $(\text{HCO}_3^- + \text{SO}_4^{2-})/(\text{Ca}^{2+} + \text{Mg}^{2+})$ (Figure 7C), implying the occurrence of ion exchange. It is clear that the contents of Ca^{2+} and SO_4^{2-} in natural water commonly depended on the dissolution of gypsum and precipitated processes, as shown in the equation of CaSO_4

TABLE 3 | Cation and silica geothermometry of hot waters from the Xifeng geothermal field.

Sample NO.	T(Na-K) [Ⓢ]	Quartz, no steam loss (conductive) [Ⓢ]	Quartz, maximum steam loss at 100 °C (adiabatic) [Ⓢ]	Chalcedony (no loss of steam) [Ⓢ]	Chalcedony (maximum steam loss) [Ⓢ]	α-Cristobalite [Ⓢ]	β-Cristobalite [Ⓢ]											
MR-1	307.37	309.16	314.99	360.55	292.27	307.65	297.25	418.19	13.51	-2.81	64.24	69.66	32.19	42.86	15.05	-29.08		
MR-2	310.25	313.28	317.57	365.29	295.09	311.41	299.81	423.67	14.18	-1.84	64.30	69.72	32.26	42.92	15.11	-29.02		
XF-1	333.57	347.34	338.41	404.58	317.95	342.33	320.49	469.36	36.68	28.32	91.36	93.50	60.71	67.45	41.21	-4.87		
XF-2	328.69	340.12	334.07	396.23	313.17	335.81	316.18	459.62	36.22	27.76	91.59	93.70	60.95	67.66	41.43	-4.66		
XF-3	334.31	348.45	339.07	405.86	318.68	343.33	321.15	470.85	36.95	28.70	91.51	93.63	60.87	67.59	41.35	-4.73		
XF-4	333.92	347.87	338.73	405.19	318.30	342.81	320.81	470.07	37.46	29.51	90.36	92.63	59.65	66.55	40.23	-5.77		
NS-1	625.48	902.36	584.19	1082.63	605.11	806.36	566.83	1316.25	33.80	18.21	53.88	60.43	21.48	33.45	5.20	-38.10		
NS-2	638.38	934.13	594.45	1123.74	617.84	830.84	577.20	1371.42	33.19	16.90	54.78	61.23	22.40	34.26	6.04	-37.32		

Notes: T(Na-K)[Ⓢ] (Fournier, 1979); T(Na-K)[Ⓢ] (Truesdell, 1976); T(Na-K)[Ⓢ] (Giggenbach and Goguel, 1988); T(Na-K)[Ⓢ] (Tonani, 1980); T(Na-K)[Ⓢ] (Neva and Neva, 1987); T(Na-K)[Ⓢ] (Armósson, 1983); T(Na-K)[Ⓢ] (Armósson, 1983); T(Na-K)[Ⓢ] (Richard et al., 1979); T(K-Mg)[Ⓢ] (Giggenbach et al., 1983); T(Na-K-Ca)[Ⓢ] (Fournier and Truesdell, 1973; where b = 4/3, if T < 100 °C; b = 1/3, if T > 100 °C); Quartz, no steam loss (conductive)[Ⓢ] (Fournier, 1977); Quartz, maximum steam loss at 100 °C (adiabatic)[Ⓢ] (Fournier, 1977); Chalcedony (no loss of steam)[Ⓢ] (Fournier, 1992); Chalcedony (maximum steam loss)[Ⓢ] (Fournier, 1977); α-Cristobalite[Ⓢ] (Fournier, 1977); β-Cristobalite[Ⓢ] (Fournier, 1977).

+ 2H₂O = Ca²⁺ + SO₄²⁻ + H₂O (Das et al., 2021). However, with influence of silicate weathering, the ratio of Ca²⁺ versus SO₄²⁻ was high than 1, except samples collected from the Xifeng hot spring (Ca²⁺/SO₄²⁻ < 1; Figure 7D). The high SO₄²⁻ in the Xifeng hot spring may be due to the dissolution of other sulphate minerals during the deeper and long-duration circulation from high-elevation SW towards low-elevation NE in the study area (Figure 4; Song et al., 2014).

Geothermal Reservoir Temperature

The Giggenbach Na-K-Mg ternary diagram is used for categorizing waters as full equilibrium, partial equilibrium, or immaturity compared with reservoir rocks (Giggenbach, 1991; Giggenbach and Goguel, 1988). As shown in Figure 9, all the sampled waters were plotted in the field of immature waters, indicating none of them were in full or partial equilibrium with the host rocks or may have mixed with shallow groundwater. It is established that only the waters with features that were fully or partially equilibrated with the host rocks can be used to obtain reliable reservoir temperatures; immature waters produce less reliable results which are usually not regarded as the real reservoir temperatures. Hence, cation geothermometers were not appropriate for the sampled waters in this study. This can be further evidenced by geo-thermometry results obtained through different Na-K geothermometers, which showed higher estimated reservoir temperatures than that of the Na-K-Ca and K-Mg geothermometers (Table 3). The inconsistent results of geothermometers containing Ca and/or Mg with that of Na-K are attributed to the mix of shallow groundwaters and/or surface waters (Figure 5; García-Soto et al., 2016). This mix made the reliability of silica-based geothermometry stronger than cation geothermometers (Pandarinath, 2011; Pandarinath and Domínguez-Domínguez, 2015; Saibi et al., 2021). The reliability of silica-based geo-thermometry can be further supported by Figure 10, which shows that the thermal and cold springs of the Xifeng geothermal field were near to the equilibrated curve of chalcedony + quartz (Giggenbach, 1991). Given that the temperatures calculated by chalcedony and cristobalite geothermometers were much lower than the real temperatures of the hot spring and wellhead, reservoir temperatures generated though the quartz (conductive and adiabatic) geothermometers were the most reliable (García-López et al., 2014). The quartz (conductive and adiabatic) geothermometers gave the average estimated reservoir temperature of 77°C. The depth of the geothermal reservoir is around 2.57 km in the Xifeng geothermal field, assuming a temperature gradient of 3°C/100 m (Song et al., 2014).

Source and Recharge of the Geothermal Fluid

Oxygen-18 (¹⁸O) and deuterium (D) contents in sampled waters from the Xifeng geothermal field were analyzed to confirm the source and circulation mechanism of geothermal fluids. On the δ¹⁸O-δD diagram (Figure 11), most samples were plotted close to

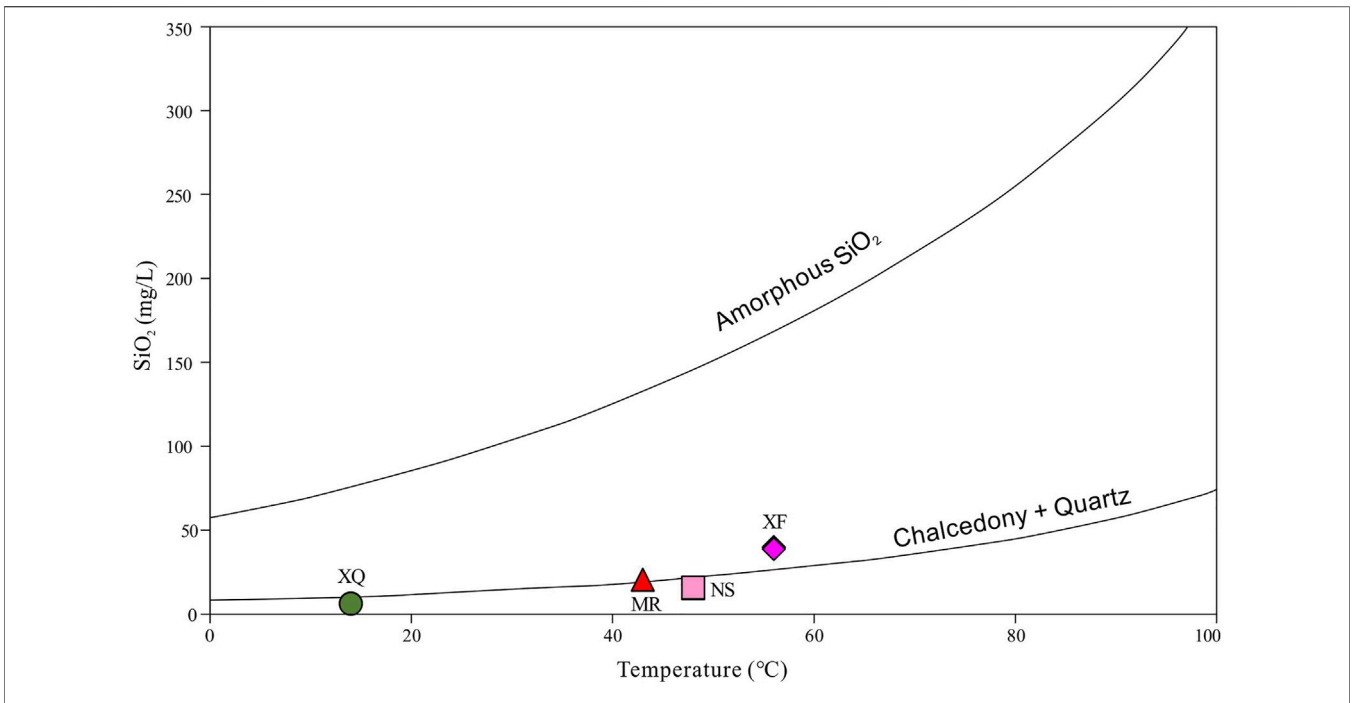


FIGURE 10 | SiO₂ concentration vs temperature plot for the samples of the Xifeng geothermal field. The amorphous SiO₂ solubility curve is from Fournier and Truesdell (1974) and chalcedony + quartz solubility is from Giggenbach (1991).

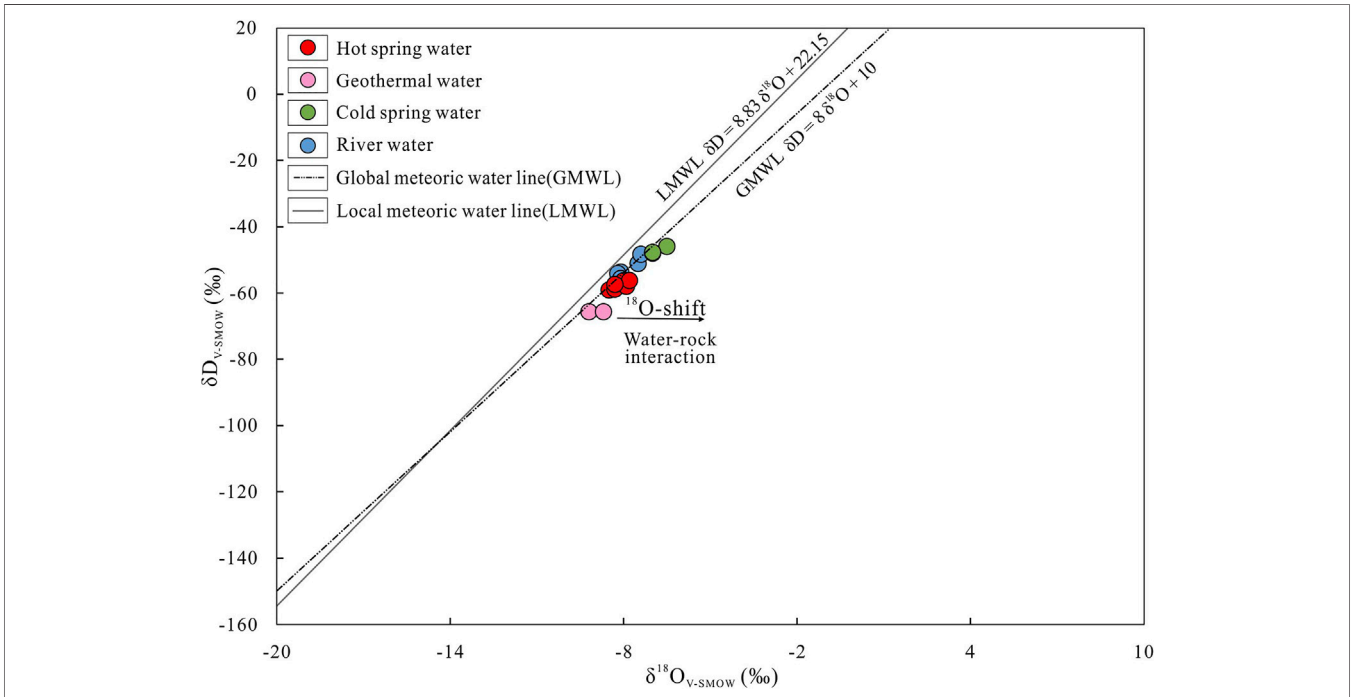
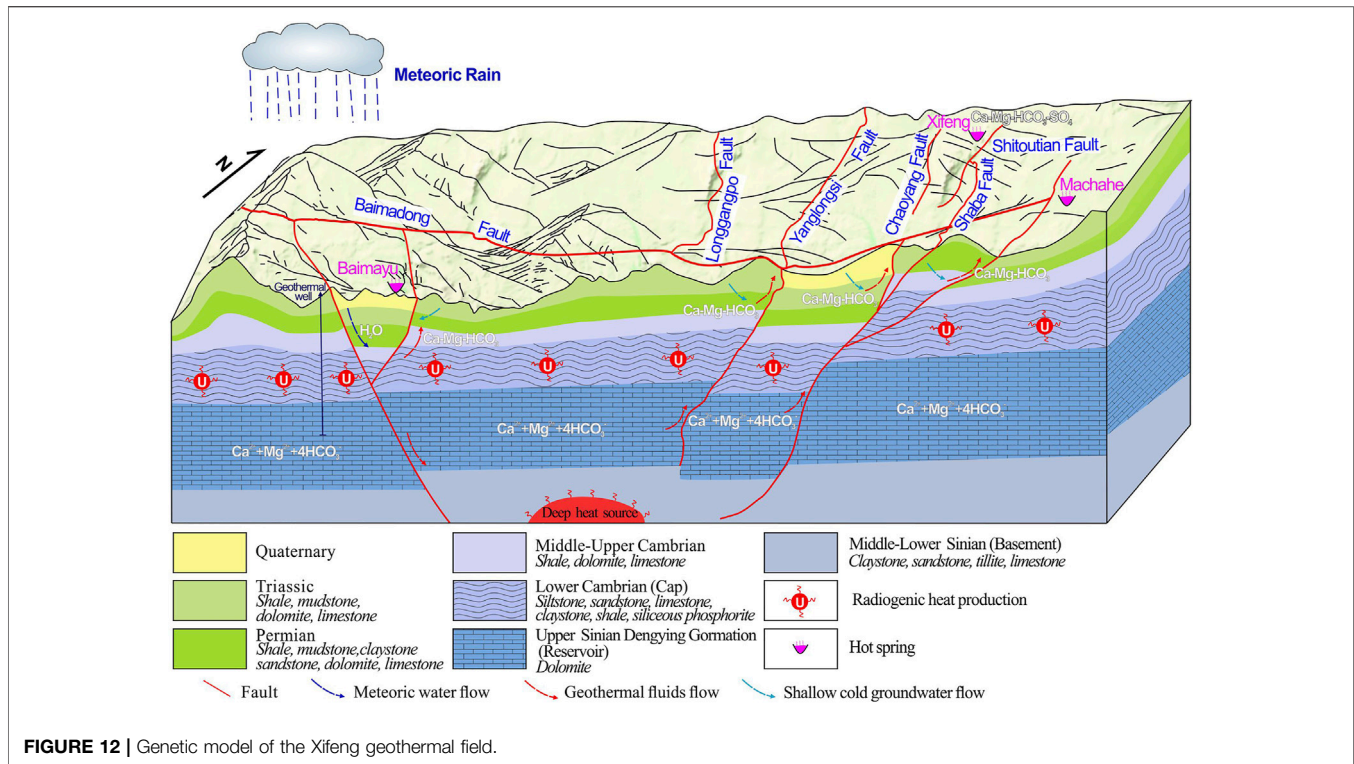


FIGURE 11 | Plot of δD vs δ¹⁸O values of water samples collected from the Xifeng geothermal field.



the local meteoric water line (LMWL: $\delta D = 8.83 \delta^{18}O + 22.15$, Zhang et al., 2005) and global meteoric water line (GMWL: $\delta D = 8 \delta^{18}O + 10$, Craig, 1961), indicating a common meteoric water origin. This is in accordance with results of the PAAS-normalized REE patterns (Figure 8) and variable characteristics of ions (Figure 4), which showed a similar source of geothermal fluids.

Craig (1961) established the δD and $\delta^{18}O$ values of precipitation relating to altitude effect, and proposed that meteoric water derived from higher elevation is gradually lighter. In Figure 11, the slightly depleted δD and $\delta^{18}O$ values of geothermal waters compared to those of local river waters testify that the recharge elevation of the former is higher than that of the latter. Generally, the recharge elevation of groundwater can be calculated in terms of the following formula:

$$H = \frac{\delta^{18}O_{gw} - \delta^{18}O_{lw}}{\text{grad}^{18}O} + h \quad (2)$$

In Eq. 2, H (m) = recharge elevation; $\delta^{18}O_{gw}$ = oxygen isotope value of groundwater; $\delta^{18}O_{lw}$ = oxygen isotope value of local meteoric water; $\text{grad}^{18}O$ (‰/km) = isotope elevation gradient of meteoric water, and h (m) = elevation of the local meteoric sampling point. The most depleted $\delta^{18}O$ value (−9.2‰) in the geothermal samples was regarded as the $\delta^{18}O_{gw}$ to minimize the positive isotopic shift effect in this study. The average oxygen isotope value (−7.7‰) of surface meteoric water obtained in this study was used as $\delta^{18}O_{lw}$. Hence, the recharge elevation was calculated to be 1,583 m as the $\delta^{18}O$ vertical gradient in Guizhou was assumed to be −3.1‰/km (Yu et al., 1984), and with the

elevation of local meteoric sampling point at 1,100 m. Combined with the geological setting, this result is reasonable as the sampling elevation is around 1,250 m for the samples collected from southwest and 750 m for those from northeast and southeast of the geothermal field.

Forming Mechanisms for the Xifeng Geothermal Field

The formation of the Xifeng geothermal field resulted from recharge, deep circulation, and secondary rising meteoric water along the faults. Based on the topographic features and geological conditions (Figures 1, 2), we propose the basic conceptual model for the genesis of the Xifeng geothermal system, as illustrated in Figure 12 and discussed.

Results of stable isotopes and geology revealed that the local meteoric water from the surrounding mountains seemed to infiltrate to depth through faults and crack zones and were the dominant recharge source for the geothermal system. Sedimentary rocks of Lower Cambrian Jindingshan, Mingxinsi, and Niutitang formations overlie the Upper Sinian Dengying reservoir units and act as cap rock (Figure 1C). Moreover, the black shale of the lower Cambrian Niutitang Formation in South China is well known to be enriched in radioactive heat-producing uranium elements, which are 10 and 6–20 times the content compared with that of crustal sedimentary rocks and the crust, respectively (Coveney and Nansheng, 1991; Ni et al., 2012; Pi et al., 2013; Yang et al., 2013; Pagès et al., 2018; Li et al., 2019). At Xifeng, the average U, Th, and K

contents for the black shale of the Niutitang Formation is 32.61 ($\mu\text{g/g}$), 13.25 ($\mu\text{g/g}$), and 1.86 (%), respectively (Chen 2005; Pi et al., 2013). Generally, the radioactive heat production can be calculated via the formula of $A = 0.01\rho(9.52C_U + 2.56C_{Th} + 3.48C_K)$ (Rybach, 1976). Where A ($\mu\text{W/m}^3$) refers to radioactive heat production, ρ (g/cm^3) is the rock density, C_U ($\mu\text{g/g}$), C_{Th} ($\mu\text{g/g}$), and C_K (%) are the U, Th, and K concentrations, respectively. Thereby, the heat production potential of the lower Cambrian Niutitang Formation in the study area is calculated to be $9.57 \mu\text{W/m}^3$ with the rock density of 2.728 (Zhao et al., 1995). This value is higher than the average heat production of the continental crust ($\sim 1 \mu\text{W/m}^3$; Waples, 2001) and can be regarded as an effective radiogenic heat source (Paternoster et al., 2017). Hence, except for the role of cap rock, the Niutitang Formation also served as a heat source due to the producing of radioactive heat (Figure 12). Furthermore, since the multi-period (especially in Yanshanian and Himalayan) active strike-slip of the Baimadong fault and Neoid active faults (e.g., Shaba, Chaoyang, and Shitoutian faults; Figure 1B) are well developed within the tectonic system of the Xifeng geothermal field, the tectonic frictional heat is speculated to act as a supplementary heat source due to the mechanical friction produced along the faults during deformation (Mase and Smith, 1987; He et al., 2014; Song et al., 2014; Zhu, 2016). Moreover, these deep large scale faults also connect to the deep earth and act as a heat transporting channel for deep heat (Figure 12; He et al., 2014; Li and Shen, 2014; Song et al., 2014; Li et al., 2019; Li J. et al., 2021). The existence of acid magmatic intrusion material under the central Guizhou uplift can be considered as the deep heat source, evidenced by the available geophysical information (Zhang et al., 2017).

Once the meteoric water was warmed up, it would interact with the host rocks. The interaction between water and Sinian dolomites is the dominant process for the formation of Ca-Mg- HCO_3 type waters in the Xifeng geothermal field. Moreover, the silicate weathering and ion exchange are also responsible for the formation of geothermal fluids in the Xifeng area. As to the Ca-Mg- HCO_3 - SO_4 type in the Xifeng hot spring, it may be due to the dissolution of other sulphate minerals during the deeper, and long-duration circulation from high-elevation SW (i.e., 1,250 m, Baimadong area) towards low-elevation NE (i.e., 750 m, Xifeng area) in the study area (Figure 12; Song et al., 2014). This is consistent with the results of recharge elevation and geological setting.

Then finally, as the deep-infiltrated waters experienced considerable deep circulation, the geothermal fluids rose again along the main ENE-SE, NE-SE, and NW-NE faults. Moreover, the ascending geothermal fluids were mixed with cold groundwater in the subsidiary fractures near the surface (Figure 5; Giggenbach, 1991). The tectonic and stratigraphical features at the study area are favorable for the formation of abundant geothermal resources.

CONCLUSION

The geothermal fluids in the Xifeng geothermal field are hosted in dolomite from the Sinian Dengying Formation, and are capped by sedimentary rocks of the lower Cambrian Jindingshan, Mingxinsi, and Niutitang formations. Radiogenic heat, deep heat, and tectonic frictional heat serve as heat sources for the formation of the large geothermal system. The reservoir temperature is estimated to be 77°C . D-O isotopic studies indicate that the Xifeng geothermal system is recharged by meteoric water from higher elevations at 1,583 m from SW to NE. It is the water-dolomite interactions that lead to the formation of the alkaline Ca-Mg- HCO_3 type geothermal fluids. This is consistent with the research results of the REE, whose accumulation characteristics and positive Eu anomaly are inherited from host feldspar-bearing dolomites through the water-rock interaction. The high SO_4 in the Xifeng hot spring are attributed to the deeper and long-duration circulation of waters from SW towards NE. Ternary relationships among major anions indicate that a mix of cold groundwater to the ascending geothermal fluids occurred when they migrated along the main faults near the surface. Taken together, the Xifeng geothermal system should be assigned as a faults-controlling and deeply circulating meteoric water of low-temperature category.

DATA AVAILABILITY STATEMENT

The original contributions presented in the study are included in the article/Supplementary Material, further inquiries can be directed to the corresponding author.

AUTHOR CONTRIBUTIONS

YL wrote the manuscript with the support of the listed authors. All authors have made a substantial, direct, and intellectual contribution to the work and approved it for publication.

FUNDING

This study was financially supported by the National Natural Science Foundation of China (No. 42002299) and the Project of Chinese Academy of Geological Sciences (No. JKY202018).

ACKNOWLEDGMENTS

We appreciate the kind help of Professor Hansheng Long from the Guizhou Institute of Technology on the field trip. The constructive comments made by the editor and anonymous reviewers are greatly thanked.

REFERENCES

- Adams, S., Titus, R., Pietersen, K., Tredoux, G., and Harris, C. (2001). Hydrochemical Characteristics of Aquifers Near Sutherland in the Western Karoo, South Africa. *J. Hydrol.* 241 (1-2), 91–103. doi:10.1016/S0022-1694(00)00370-x
- Arnórsson, S. (1983). Chemical Equilibria in Icelandic Geothermal Systems. Implications for Chemical Geothermometry Investigations. *Geothermics* 12, 119–128. doi:10.1016/0375-6505(83)90022-6
- Belkhir, L., and Narany, T. S. (2015). Using Multivariate Statistical Analysis, Geostatistical Techniques and Structural Equation Modeling to Identify Spatial Variability of Groundwater Quality. *Water Resour. Manag.* 29 (6), 2073–2089. doi:10.1007/s11269-015-0929-7
- Bob, M., Abd Rahman, N., Taher, S., and Elamin, A. (2015). Multi-objective Assessment of Groundwater Quality in Madinah City, Saudi Arabia. *Water Qual. Expo. Health* 7 (1), 53–66. doi:10.1007/s12403-014-0112-z
- Cai, X. L., Zhang, C. J., Guo, J. B., Wu, D., Fan, X., and Yang, M. J. (2018). Geothermal Water Genetic Analysis in Kaiyang Phosphate Mine West Limb, Guizhou. *Coal Geology. China* 30 (6), 101–104. doi:10.3969/j.issn.1674-1803.2018.06.20
- Carter, A., Roques, D., Bristow, C., and Kinny, P. (2001). Understanding Mesozoic Accretion in Southeast Asia: Significance of Triassic Thermotectonism (Indosinian Orogeny) in Vietnam. *Geol.* 29, 211–214. doi:10.1130/0091-7613(2001)029<0211:umaisa>2.0.co;2
- Chen, L. (2005). *Sedimentology and Geochemistry of the Early Cambrian Black Rock Series in the Human-Guizhou Area, China*. A Dissertation Submitted for the Degree of Doctor of Science of the Chinese Academy of Sciences and for the Diploma of the Institute of Geochemistry, 53–79. (in Chinese with English abstract).
- Chen, Y.-J., Santosh, M., Somerville, I., and Chen, H.-Y. (2014). Indosinian Tectonics and Mineral Systems in China: An Introduction. *Geol. J.* 49, 331–337. doi:10.1002/gj.2619
- Cheng, Y., Pang, Z., Di, Q., Chen, X., and Kong, Y. (2021). Three-dimensional Resistivity Structure in the Hydrothermal System beneath Ganzi Basin, Eastern Margin of Tibetan Plateau. *Geothermics* 93, 102062. doi:10.1016/j.geothermics.2021.102062
- Coveney, R. M., Jr., and Nansheng, C. (1991). Ni-Mo-PGE-Au-rich Ores in Chinese Black Shales and Speculations on Possible Analogues in the United States. *Mineral. Deposita* 26, 83–88. doi:10.1007/bf00195253
- Craig, H. (1961). Isotopic Variations in Meteoric Waters. *Science* 133 (3465), 1702–1703. doi:10.1126/science.133.3465.1702
- Das, P., Maya, K., and Padmalal, D. (2021). Hydrochemistry, Geothermometry and Origin of the Low Temperature thermal Springs of South Konkan Region, India. *Geothermics* 90, 101997. doi:10.1016/j.geothermics.2020.101997
- Duo, J. (2003). The Basic Characteristics of the Yangbajing Geothermal Field? A Typical High Temperature Geothermal System. *Eng. Sci.* 1, 42–47. doi:10.3969/j.issn.1009-1742.2003.01.008
- Fournier, R. O. (1977). Chemical Geothermometers and Mixing Models for Geothermal Systems. *Geothermics* 5, 41–50. doi:10.1016/0375-6505(77)90007-4
- Fournier, R. O. (1979). Geochemical and Hydrologic Considerations and the Use of Enthalpy-Chloride Diagrams in the Prediction of Underground Conditions in Hot-spring Systems. *J. Volcanology Geothermal Res.* 5, 1–16. doi:10.1016/0377-0273(79)90029-5
- Fournier, R. O., and Truesdell, A. H. (1973). An Empirical Na-K-Ca Geothermometer for Natural Waters. *Geochimica et Cosmochimica Acta* 37, 1255–1275. doi:10.1016/0016-7037(73)90060-4
- Fournier, R. O., and Truesdell, A. H. (1974). Geochemical Indicators of Subsurface Temperature - Part 2. *USGS J. Res.* 2, 263–270. doi:10.3133/ofr741032
- Fournier, R. O. (1992). Water Geothermometers Applied to Geothermal Energy. F. D'Amore (Coordinator). *Application of Geochemistry in Geothermal Reservoir Development*. UNITAR/UNDP, Vial del Corso, Italy, 37–69.
- García-López, C. G., Pandarinath, K., and Santoyo, E. (2014). Solute and Gas Geothermometry of Geothermal Wells: A Geochemometrics Study for Evaluating the Effectiveness of Geothermometers to Predict Deep Reservoir Temperatures. *Int. Geology. Rev.* 56, 2015–2049. doi:10.1080/00206814.2014.984352
- García-Soto, A. Y., Pandarinath, K., Marrero-Ochoa, J. E., and Díaz-Gómez, C. (2016). Solute Geothermometry of Cerro Prieto and Los Hornos Geothermal Fields, Mexico: Considerations on Chemical Characteristics of Thermal Water. *Arab. J. Geosci.* 9, 517. doi:10.1007/s12517-016-2529-0
- Giggenbach, W. F. (1991). "Chemical Techniques in Geothermal Exploration," in *Application of Geochemistry in Resources Development* (UNITAR/UNDP Guidebook), 119–144.
- Giggenbach, W. F., and Glover, R. B. (1992). Tectonic Regime and Major Processes Governing the Chemistry of Water and Gas Discharges from the Rotorua Geothermal Field, New Zealand. *Geothermics* 21, 121–140. doi:10.1016/0375-6505(92)90073-i
- Giggenbach, W. F., and Goguel, R. L. (1988). *Collection and Analysis of Geothermal and Volcanic Water and Gas Discharges*. Department of Scientific and Industrial Research, Chemistry Division: Petone. 4th ed. (New Zealand). Report No.: CD 2401.
- Giggenbach, W. F., Gonfiantini, R., Jangi, B. L., and Truesdell, A. H. (1983). Isotopic and Chemical Composition of Parbati Valley Geothermal Discharges, North-West Himalaya, India. *Geothermics* 12 (2-3), 199–222. doi:10.1016/0375-6505(83)90030-5
- Guo, Q. H., Wang, Y. X., and Liu, W. (2007). Major Hydrogeochemical Processes in the Two Reservoirs of the Yangbajing Geothermal Field, Tibet, China. *J. Volcanol. Geotherm. Res.* 166 (3–4), 255–268. doi:10.1016/j.jvolgeores.2007.08.004
- Guo, Q., Kirk Nordstrom, D., and Blaine McCleskey, R. (2014). Towards Understanding the Puzzling Lack of Acid Geothermal Springs in Tibet (China): Insight from A Comparison with Yellowstone (USA) and Some Active Volcanic Hydrothermal Systems. *J. Volcanology Geothermal Res.* 288 (1), 94–104. doi:10.1016/j.jvolgeores.2014.10.005
- Guo, Q., Liu, M., Li, J., Zhang, X., Guo, W., and Wang, Y. (2017a). Fluid Geochemical Constraints on the Heat Source and Reservoir Temperature of the Banglazhang Hydrothermal System, Yunnan-Tibet Geothermal Province, China. *J. Geochemical Exploration* 172, 109–119. doi:10.1016/j.jgexpro.2016.10.012
- Guo, Q., Planer-Friedrich, B., Liu, M., Li, J., Zhou, C., and Wang, Y. (2017b). Arsenic and Thioarsenic Species in the hot springs of the Rehai Magmatic Geothermal System, Tengchong Volcanic Region, China. *Chem. Geology* 453, 12–20. doi:10.1016/j.chemgeo.2017.02.010
- Guo, Q., and Wang, Y. (2012). Geochemistry of Hot Springs in the Tengchong Hydrothermal Areas, Southwestern China. *J. Volcanology Geothermal Res.* 215–216, 61–73. doi:10.1016/j.jvolgeores.2011.12.003
- Han, Y., Wang, G., Cravotta, C. A., III, Hu, W., Bian, Y., Zhang, Z., et al. (2013). Hydrogeochemical Evolution of Ordovician Limestone Groundwater in Yanzhou, North China. *Hydrol. Process.* 27 (16), 2247–2257. doi:10.1002/hyp.9297
- He, B., Xu, Y. G., and Wang, Y. M. (2005). Nature of the Dongwu Movement and its Temporal and Spatial Evolution. *J. China Univ. Geosci.* 30, 89–96. doi:10.3321/j.issn:1000-2383.2005.01.012
- He, W. J., Xiang, X. L., Li, Y. G., and Wu, X. J. (2014). Genesis and Hydrochemical Characteristics of Xinluo, Guizhou Province. *Ground water* 36 (5), 39–40. doi:10.3969/j.issn.1004-1184.2014.05.013
- Huang, T. K. (1945). On Major Tectonic Forms of China. *J. Geol.* 55, 59–60. doi:10.1086/625397
- Ji, Q. (2015). *The Hydrogeochemical Characteristics and Genesis Research of Xifeng Hot Springs in Guizhou*. A Dissertation Submitted for the Degree of Master of Chengdu University of Technology, 1–51. (in Chinese with English abstract).
- Jian, P., Liu, D., Kröner, A., Zhang, Q., Wang, Y., Sun, X., et al. (2009). Devonian to Permian Plate Tectonic Cycle of the Paleo-Tethys Orogen in Southwest China (II): Insights from Zircon Ages of Ophiolites, Arc/back-Arc Assemblages and Within-Plate Igneous Rocks and Generation of the Emeishan CFB Province. *Lithos* 113, 767–784. doi:10.1016/j.lithos.2009.04.006
- Katz, B. G., Coplen, T. B., Bullen, T. D., and Davis, J. H. (1997). Use of Chemical and Isotopic Tracers to Characterize the Interactions between Ground Water and Surface Water in Mantled Karst. *Groundwater* 35 (6), 1014–1028. doi:10.1111/j.1745-6584.1997.tb00174.x
- Lewis, A. J., Palmer, M. R., and Kemp, A. J. (1994). Variations of the Rare Earth Element Abundances in Hydrothermal Waters from the Yellowstone Hydrothermal System, Wyoming, USA. *Mineralogical Mag.* 58A, 525–526. doi:10.1180/minmag.1994.58a.2.11

- Li, D. W., and Wang, Y. X. (2015). Major Issues of Research and Development of Hot Dry Rock Geothermal Energy. *Earth Sci.* 40 (11), 1858–1869. doi:10.3799/dqkx.2015.166
- Li, J., Sagoe, G., Wang, X., and Yang, Z. (2021a). Assessing the Suitability of Lithium-Related Geothermometers for Estimating the Temperature of Felsic Rock Reservoirs. *Geothermics* 89, 101950. doi:10.1016/j.geothermics.2020.101950
- Li, J., Yang, G., Sagoe, G., and Li, Y. (2018). Major Hydrogeochemical Processes Controlling the Composition of Geothermal Waters in the Kangding Geothermal Field, Western Sichuan Province. *Geothermics* 75, 154–163. doi:10.1016/j.geothermics.2018.04.008
- Li, Y. Y., Zhang, C. J., Chi, G. X., Duo, J., Li, Z. H., and Song, H. (2019). Black and Red Alterations Associated with the Baimadong Uranium Deposit (Guizhou, China): Geological and Geochemical Characteristics and Genetics Relationship with Uranium Mineralization. *Ore Geol. Rev.* 111, 102981. doi:10.1016/j.oregeorev.2019.102981
- Li, Y. Y., Zhang, C. J., Duo, J., Zhang, F. F., Song, H., Zhang, B. J., et al. (2021b). Genesis of the Baimadong Carbonate-Hosted Uranium Deposit, Guizhou, SW China: Constrains from Geology, Fluid Inclusions, and C-O Isotopes. *Ore Geol. Rev.* 139, 104487. doi:10.1016/j.oregeorev.2021.104487
- Li, Z. S., and Shen, X. D. (2014). Genesis of the Xinluo Geothermal Well in Xifeng, Guizhou Province. *Geology. Exploration* 50 (6), 1155–1159. (in Chinese with English abstract).
- Ling, K.-Y., Zhu, X.-Q., Tang, H.-S., and Li, S.-X. (2017). Importance of Hydrogeological Conditions during Formation of the Karstic Bauxite Deposits, Central Guizhou Province, Southwest China: A Case Study at Lindai Deposit. *Ore Geology. Rev.* 82, 198–216. doi:10.1016/j.oregeorev.2016.11.033
- Ling, K.-Y., Zhu, X.-Q., Tang, H.-S., Wang, Z.-G., Yan, H.-W., Han, T., et al. (2015). Mineralogical Characteristics of the Karstic Bauxite Deposits in the Xiwen Ore Belt, Central Guizhou Province, Southwest China. *Ore Geology. Rev.* 65, 84–96. doi:10.1016/j.oregeorev.2014.09.003
- Liu, P. (2001). Discussion on the Metallogenic Setting of the Qianzhong-Yu'nan Bauxite in Guizhou and its Genesis. *Guizhou Geol.* 18, 238–243. doi:10.3969/j.issn.1000-5943.2001.04.006
- Long, Y., Chi, G., Liu, J., Jin, Z., and Dai, T. (2017). Trace and Rare Earth Elements Constraints on the Sources of the Yunfeng Paleo-Karstic Bauxite Deposit in the Xiwen-Qingzhen Area, Guizhou, China. *Ore Geology. Rev.* 91, 404–418. doi:10.1016/j.oregeorev.2017.09.014
- Long, Y., Chi, G., Liu, J., Zhang, D., and Song, H. (2018). Uranium Enrichment in a Paleo-Karstic bauxite deposit, Yunfeng, SW China: Mineralogy, Geochemistry, Transport - Deposition Mechanisms and Significance for Uranium Exploration. *J. Geochemical Exploration* 190, 424–435. doi:10.1016/j.gexplo.2018.04.010
- Long, Y., Lu, A., Gu, X., Chi, G., Ye, L., Jin, Z., et al. (2020). Cobalt Enrichment in A Paleo-Karstic Bauxite Deposit at Yunfeng, Guizhou Province, SW China. *Ore Geology. Rev.* 117, 103308. doi:10.1016/j.oregeorev.2019.103308
- Luo, T. (2020). *Study on the Enrichment Mechanism of H₂SiO₃ and Sr in Xifeng Water*. A Dissertation Submitted for the Degree of Master of Guizhou University, 1–69. (in Chinese with English abstract).
- Mase, C. W., and Smith, L. (1987). Effects of Frictional Heating on the Thermal, Hydrologic, and Mechanical Response of a Fault. *J. Geophys. Res.* 92 (B7), 6249–6272. doi:10.1029/jb092ib07p06249
- Mei, M. X., Ma, Y. S., Deng, J., Li, H., and Zheng, K. B. (2005). Tectonic Palaeogeographic Changes Resulting from the Caledonian Movement and the Formation of the Dianqiangui Basin: Discussion on the Deep Exploration Potential of Oil and Gas in the Dianqiangui Basin. *Earth Sci. Front.* 12, 227–236. (in Chinese with English abstract).
- Michard, G. (1979). Géothermomètres Chimiques. *Bull. de BRGM* 2, 183–189.
- Ni, S. J., Xu, Z. Q., Zhang, C. J., Song, H., and Luo, C. (2012). Uranium Metallogenesis and Ore Genesis of the Rich-Large Black Rock Series-type Uranium Deposits in Southwest China. *Adv. Earth Sci.* 27, 1035–1042. (in Chinese with English abstract).
- Nieva, D., and Nieva, R. (1987). Developments in Geothermal Energy in Mexico-part Twelve. A Cationic Geothermometer for Prospecting of Geothermal Resources. *Heat Recovery Syst. CHP* 7 (3), 243–258. doi:10.1016/0890-4332(87)90138-4
- Pagès, A., Barnes, S., Schmid, S., Coveney, R. M., Jr., Schwark, L., Liu, W. H., et al. (2018). Geochemical Investigation of the Lower Cambrian Mineralised Black Shales of South China and the Late Devonian Nick Deposit, Canada. *Ore Geol. Rev.* 94, 396–413. doi:10.1016/j.oregeorev.2018.02.004
- Pandarínath, K., and Domínguez-Domínguez, H. (2015). Evaluation of the Solute Geothermometry of Thermal Springs and Drilled Wells of La Primavera (Cerritos Colorados) Geothermal Field, Mexico: a Geochemometrics Approach. *J. South Am. Earth Sci.* 62, 109–124. doi:10.1016/j.jsames.2015.05.002
- Pandarínath, K. (2011). Solute Geothermometry of Springs and wells of the Los Azufres and Las Tres Virgenes Geothermal fields, Mexico. *Int. Geology. Rev.* 53 (9), 1032–1058. doi:10.1080/00206810903442014
- Paternoster, M., Oggiano, G., Sinisi, R., Caracausi, A., and Mongelli, G. (2017). Geochemistry of Two Contrasting Deep Fluids in the Sardinia Microplate (Western Mediterranean): Relationships with Tectonics and Heat Sources. *J. Volcanology Geothermal Res.* 336, 108–117. doi:10.1016/j.jvolgeores.2017.02.011
- Pi, D.-H., Liu, C.-Q., Shields-Zhou, G. A., and Jiang, S.-Y. (2013). Trace and Rare Earth Element Geochemistry of Black Shale and Kerogen in the Early Cambrian Niutitang Formation in Guizhou Province, South China: Constraints for Redox Environments and Origin of Metal Enrichments. *Precambrian Res.* 225, 218–229. doi:10.1016/j.precamres.2011.07.004
- Piper, A. M. (1944). A Graphic Procedure in the Geochemical Interpretation of Water-Analyses. *Trans. AGU* 25 (6), 914–928. doi:10.1029/tr025i006p00914
- Reid, A., Wilson, C. J. L., Shun, L., Pearson, N., and Belousova, E. (2007). Mesozoic Plutons of the Yidun Arc, SW China: U-Pb Geochronology and Hf Isotopic Signature. *Ore Geol. Rev.* 31, 88–106. doi:10.1016/j.oregeorev.2004.11.003
- Saibi, H., Batir, J. F., and Pocasangre, C. (2021). Hydrochemistry and Geothermometry of thermal Waters from UAE and Their Energetic Potential Assessment. *Geothermics* 92, 102061. doi:10.1016/j.geothermics.2021.102061
- Schoeller, H. (1955). *Geochemie des eaux souterraines. Revue De L'institute Francois Du Petrole* 10, 230–244.
- Şener, M. F., Şener, M., and Uysal, I. T. (2017). The Evolution of the Cappadocia Geothermal Province, Anatolia (Turkey): Geochemical and Geochronological Evidence. *Hydrogeol. J.* 25, 2323–2345. doi:10.1007/s10040-017-1613-1
- Song, X. Q., Duan, Q. S., Meng, F. T., and Cao, Z. D. (2014). Geological Genesis Analysis of the Xifeng Hot Spring in Guizhou. *Geol. Sci. Tech. Inf.* 33 (5), 216–220. (in Chinese with English abstract).
- Sverjensky, D. A. (1984). Europium Redox Equilibria in Aqueous Solution. *Earth Planet. Sci. Lett.* 67, 70–78. doi:10.1016/0012-821X(84)90039-6
- Taylor, H. P., Jr. (1977). Water/rock Interactions and the Origin of H₂O in Granitic Batholiths. *J. Geol. Soc.* 133, 509–558. doi:10.1144/gsjgs.133.6.0509
- Tian, J., Pang, Z., Guo, Q., Wang, Y., Li, J., Huang, T., et al. (2018). Geochemistry of Geothermal Fluids with Implications on the Sources of Water and Heat Recharge to the Rekeng High-Temperature Geothermal System in the Eastern Himalayan Syntax. *Geothermics* 74, 92–105. doi:10.1016/j.geothermics.2018.02.006
- Tonani, F. B. (1980). "Some Remarks on the Application of Geochemical Techniques in Geothermal Exploration," in *Advances in European Geothermal Research*. Editors A. S. Strub and P. Ungemach (Dordrecht: Springer), 428–443. doi:10.1007/978-94-009-9059-3_38
- Truessedell, A. H. (1976). "Summary of Section III: Geochemical Techniques in Exploration," in *Proceedings of Second United Nations Symposium on the Development and Use of Geothermal Resources*, San Francisco, May 20–29 (Lawrence Berkeley Laboratory), 53–89. U. S. Government Printing Office.
- Wang, G. L., Zhang, W., Liang, J. Y., Lin, W. J., Liu, Z. M., and Wang, W. L. (2017a). Evaluation of Geothermal Resources Potential in China. *Acta Geoscientia Sinica* 38 (4), 449–459. doi:10.3975/cagsb.2017.04.02
- Wang, H., and Mo, X. (1995). An Outline of the Tectonic Evolution of China. *Episodes* 18, 6–16. doi:10.18814/epiugs/1995/v18i1.2/003
- Wang, H. S., Cai, X. L., Lei, L. F., and Liu, C. B. (2017b). Analysis on Structural Characteristics in Yangshui Mining Area of Kaiyang Phosphate Mine, Central Guizhou. *Geology. Chem. Minerals* 39 (2), 90–95. (in Chinese with English abstract).
- Wang, X., Wang, G., Lu, C., Gan, H., and Liu, Z. (2018). Evolution of Deep Parent Fluids of Geothermal Fields in the Nimu-Nagchu Geothermal Belt, Tibet, China. *Geothermics* 71, 118–131. doi:10.1016/j.geothermics.2017.07.010
- Wang, Y., Hu, S., Wang, Z., Jiang, G., Hu, D., Zhang, K., et al. (2019a). Heat Flow, Heat Production, Thermal Structure and its Tectonic Implication of the

- Southern Tan-Lu Fault Zone, East-Central China. *Geothermics* 82, 254–266. doi:10.1016/j.geothermics.2019.06.007
- Wang, Y., Pang, Z., Hao, Y., Fan, Y., Tian, J., and Li, J. (2019b). A Revised Method for Heat Flux Measurement with Applications to the Fracture-Controlled Kangding Geothermal System in the Eastern Himalayan Syntaxis. *Geothermics* 77, 188–203. doi:10.1016/j.geothermics.2018.09.005
- Waples, D. W. (2001). A New Model for Heat Flow in Extensional Basins: Radiogenic Heat, Asthenospheric Heat, and the McKenzie Model. *Nat. Resour. Res.* 10, 3. doi:10.1023/a:1012521309181
- Yang, E. L., Lu, X. B., Bao, M., Luo, J. J., and Hu, Q. C. (2013). Enrichment and Origin of Some Trace Elements in Black Shales from the Early Cambrian in Eastern Guizhou Province. *Adv. Earth Sci.* 28, 1160–1169. doi:10.11867/j.issn.1001-8166.2013.10.1160
- Yang, R. K., Luo, W., Pei, Y. W., and Wang, Q. (2018). Distribution and Fluids Hydrochemistry Characteristics of Hydrothermal Resources in Guizhou Province. *Geol. Surv. China* 5 (2), 38–44. doi:10.19388/j.zgdzdc.2018.02.06
- Yu, J., Zhang, H., Yu, F., and Liu, D. (1984). Oxygen and Hydrogen Isotopic Compositions of Meteoric Waters in the Eastern Part of Xizang. *Chin. J. Geochem.* 3 (2), 93–101. doi:10.1007/BF03179285
- Zhang, X. P., Sun, W. Z., and Liu, J. M. (2005). Stable Isotopes in Precipitation in the Vapor Transport Path in Kunming of Southwest China. *Resour. Environ. Yangtze Basin* 14 (5), 665–669. doi:10.1007/s11769-005-0033-7
- Zhang, X. Q., Huang, K. P., Yuan, L., Shen, X. D., and Zheng, M. R. (2017). Prospecting Potential Analysis and Uranium Mineralization Control of Deep Fracture and Interlayer Detachment Structure System of Baimadong Uranium deposit in Guizhou. *Guizhou Geol.* 34, 237–243. doi:10.3969/j.issn.1000-5943.2017.04.004
- Zhang, Y., Tan, H., Zhang, W., Wei, H., and Dong, T. (2016). Geochemical Constraint on Origin and Evolution of Solutes in Geothermal Springs in Western Yunnan, China. *Geochemistry* 76, 63–75. doi:10.1016/j.chemer.2015.11.002
- Zhao, P., Wang, J. Y., Wang, J. A., and Luo, D. G. (1995). Characteristics of Heat Production Distribution in SE China. *Acta Petrologica Sinica* 11 (3), 292–305.
- Zheng, H. R., Luo, J., Zhang, Y., Feng, J. Y., Zeng, Y., and Wang, M. C. (2021). Geological Characteristics and Distribution of Granite Geothermal Reservoir in Southeast Coastal Areas in China. *Front. Earth Sci.* 9, 683–696. doi:10.3389/feart.2021.683696
- Zhou, M.-F., Yan, D.-P., Kennedy, A. K., Li, Y., and Ding, J. (2002). SHRIMP U-Pb Zircon Geochronological and Geochemical Evidence for Neoproterozoic Arc-Magmatism along the Western Margin of the Yangtze Block, South China. *Earth Planet. Sci. Lett.* 196, 51–67. doi:10.1016/s0012-821x(01)00595-7
- Zhu, P. P. (2016). Frictional Strength and Heat Flow of Southern San Andreas Fault. *J. Seismol.* 20 (1), 291–304. doi:10.1007/s10950-015-9527-7

Conflict of Interest: The handling editor declared a shared affiliation with the authors JD and CZ at the time of review

The authors declare that the research was conducted in the absence of any commercial or financial relationships that could be construed as a potential conflict of interest.

Publisher's Note: All claims expressed in this article are solely those of the authors and do not necessarily represent those of their affiliated organizations, or those of the publisher, the editors and the reviewers. Any product that may be evaluated in this article, or claim that may be made by its manufacturer, is not guaranteed or endorsed by the publisher.

Copyright © 2021 Li, Dor, Zhang, Wang, Zhang, Zhang and Xing. This is an open-access article distributed under the terms of the Creative Commons Attribution License (CC BY). The use, distribution or reproduction in other forums is permitted, provided the original author(s) and the copyright owner(s) are credited and that the original publication in this journal is cited, in accordance with accepted academic practice. No use, distribution or reproduction is permitted which does not comply with these terms.